Article

Maize smart-canopy architecture enhances yield at high densities

https://doi.org/10.1038/s41586-024-07669-6

Received: 23 January 2023

Accepted: 4 June 2024

Published online: 12 June 2024

Check for updates

Jinge Tian[1,2,10], Chenglong Wang[1,10], Fengyi Chen[1,10], Wenchao Qin[1], Hong Yang[1], Sihang Zhao[3], Jinliang Xia[1], Xian Du[1], Yifan Zhu[1], Lishuan Wu[1], Yan Cao[4], Hong Li[4], Junhong Zhuang[4], Shaojiang Chen[5], Huayuan Zhang[6], Qiuyue Chen[7], Mingcai Zhang[8], Xing Wang Deng[9], Dezhi Deng[6], Jigang Li[4] ✉ & Feng Tian[1,3] ✉

Increasing planting density is a key strategy for enhancing maize yields[1–3]. An ideotype for dense planting requires a 'smart canopy' with leaf angles at different canopy layers differentially optimized to maximize light interception and photosynthesis[4–6], among other features. Here we identified *leaf angle architecture of smart canopy 1* (*lac1*), a natural mutant with upright upper leaves, less erect middle leaves and relatively flat lower leaves. *lac1* has improved photosynthetic capacity and attenuated responses to shade under dense planting. *lac1* encodes a brassinosteroid C-22 hydroxylase that predominantly regulates upper leaf angle. Phytochrome A photoreceptors accumulate in shade and interact with the transcription factor RAVL1 to promote its degradation via the 26S proteasome, thereby inhibiting activation of *lac1* by RAVL1 and decreasing brassinosteroid levels. This ultimately decreases upper leaf angle in dense fields. Large-scale field trials demonstrate that *lac1* boosts maize yields under high planting densities. To quickly introduce *lac1* into breeding germplasm, we transformed a haploid inducer and recovered homozygous *lac1* edits from 20 diverse inbred lines. The tested doubled haploids uniformly acquired smart-canopy-like plant architecture. We provide an important target and an accelerated strategy for developing high-density-tolerant cultivars, with *lac1* serving as a genetic chassis for further engineering of a smart canopy in maize.

Global climate change, reductions in arable land and the growing world population pose grand challenges for food security and sustainable agriculture. To meet the increasing demands for food, global agricultural production needs to be doubled by 2050[7,8]. Maize (*Zea mays*) is the most produced crop in the world, and serves as a major source of human food, livestock feed and industrial materials. Over the past few decades, continuous increases in planting densities have had a key role in yield gains in the USA—from around 30,000 plants per hectare in the 1930s to more than 80,000 plants per hectare currently[1–3]. Similar trends were also observed in other countries, including China[9]. This success is largely attributed to the development of high-density-tolerant maize cultivars.

Optimal plant architecture is a prerequisite for adapting maize to dense planting. Leaf angle is a major trait that determines plant architecture. Upright leaf angles reduce mutual shading and increase solar-irradiation penetration, thus improving photosynthetic efficiency at the population level to ultimately enhance grain yield under dense planting[3,4,10]. More upright leaves are selected in contemporary maize breeding[3,11]. Within dense canopies typical of the maize field, leaves at different canopy layers receive distinct qualities and quantities of sunlight, which requires differential leaf orientation to maximize light interception and photosynthesis. Therefore, plant architecture ideal for dense planting does not simply require uniform upright leaf angles across the entire canopy, but instead needs an optimized distribution of leaf angles at different canopy layers. Ort et al.[5] proposed an ideotype called a smart canopy, which includes optimized plant architecture together with improved biochemical features in leaves such as differential Rubisco catalytic capacities and photosystems across the plant[5]. In terms of architecture, a smart canopy features upright leaves in the upper canopy, less erect leaves in the middle canopy and relatively flat leaves in the lower canopy[4–6]. Such canopy architecture would enable light to spread more evenly within a dense canopy, minimizing light saturation of the upper leaves and light starvation of the lower leaves[4–6].

[1]State Key Laboratory of Plant Environmental Resilience, Frontiers Science Center for Molecular Design Breeding, National Maize Improvement Center, Center for Crop Functional Genomics and Molecular Breeding, Key Laboratory of Biology and Genetic Improvement of Maize (MOA), Beijing Key Laboratory of Crop Genetic Improvement, China Agricultural University, Beijing, China. [2]Maize Research Institute, Beijing Academy of Agriculture and Forestry Sciences (BAAFS), Beijing, China. [3]Sanya Institute of China Agricultural University, Sanya, China. [4]State Key Laboratory of Plant Environmental Resilience, Center for Crop Functional Genomics and Molecular Breeding, College of Biological Sciences, China Agricultural University, Beijing, China. [5]National Maize Improvement Center of China, Key Laboratory of Crop Heterosis and Utilization (MOE), China Agricultural University, Beijing, China. [6]Hainan Aoyu Biotechnology, Sanya, China. [7]Department of Crop and Soil Sciences, North Carolina State University, Raleigh, NC, USA. [8]State Key Laboratory of Plant Environmental Resilience, Engineering Research Center of Plant Growth Regulator, Ministry of Education, College of Agronomy and Biotechnology, China Agricultural University, Beijing, China. [9]Peking University Institute of Advanced Agricultural Sciences, Shandong Laboratory of Advanced Agricultural Sciences at Weifang, Weifang, China. [10]These authors contributed equally: Jinge Tian, Chenglong Wang, Fengyi Chen. ✉e-mail: jigangli@cau.edu.cn; ft55@cau.edu.cn

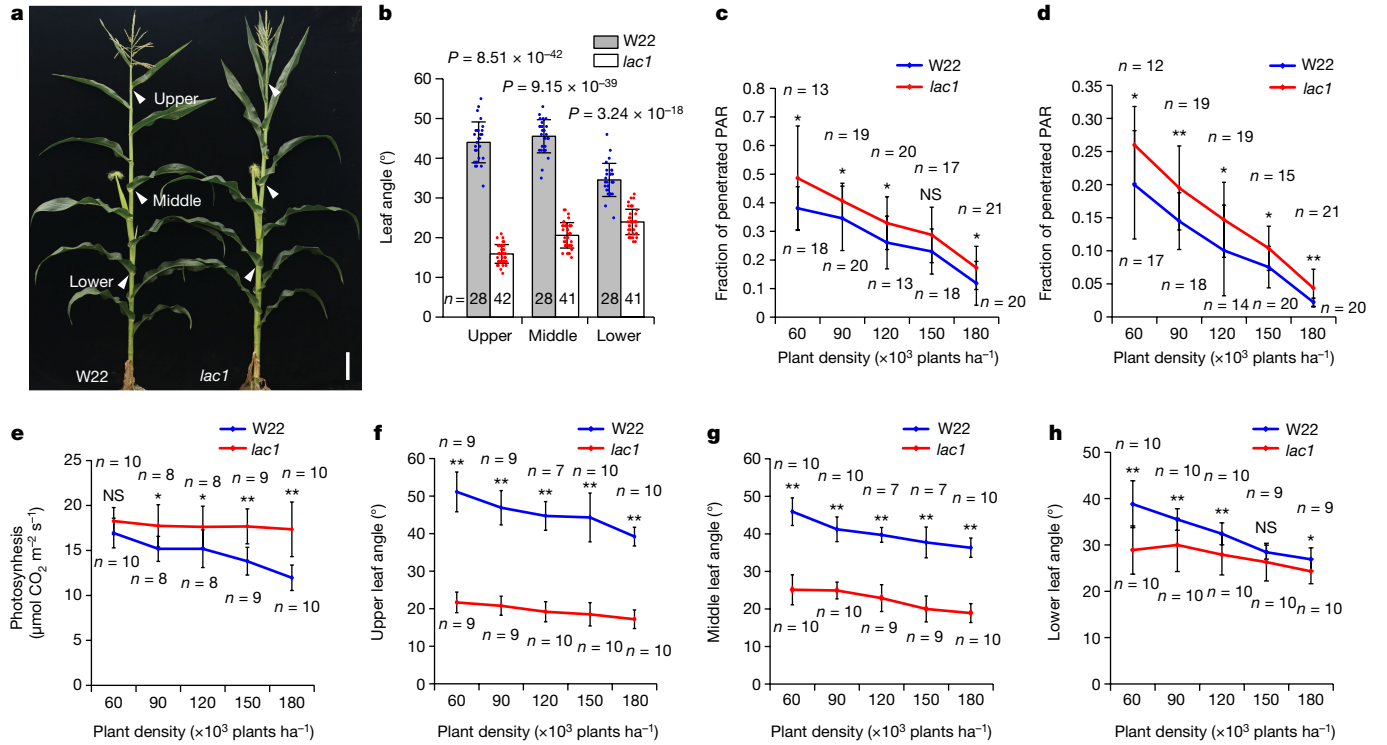

Fig. 1 | The *lac1* mutant displays smart-canopy-like plant architecture. **a**, Phenotypes of *lac1* and wild-type (W22) plants. White arrows indicate the lower, middle and upper leaves from which leaf angle was scored. Scale bar, 16 cm. **b**, Comparison of the upper, middle and lower leaf angles between *lac1* and W22 under a planting density of 82,500 plants per hectare. **c**,**d**, Comparison of light penetration at the layer of the ear leaf (**c**) and the layer at 10 cm above the soil surface (**d**) between *lac1* and W22 under different planting densities. PAR, photosynthetically active radiation. Fraction of penetrated PAR is calculated as the ratio of PAR measured at different canopy layers to PAR measured above the canopy. **e**, Comparison of net photosynthesis of the ear leaf between *lac1* and W22 under different planting densities. **f**–**h**, Comparison of the upper leaf angle (**f**), middle leaf angle (**g**) and lower leaf angle (**h**) between *lac1* and W22 under different planting densities. Data are mean ± s.d. *n* represents numbers of biologically independent samples. In **b**–**h**, a two-tailed Student's *t*-test was used to determine *P* values (see Source Data). $^{*}P < 0.05$. $^{**}P < 0.01$; NS, not significant.

Mutant analysis, quantitative trait locus (QTL) cloning and comparative genomic studies have identified a series of genes that control maize leaf angle[4,12]. However, most of these leaf angle genes tend to have a canopy-wide effect, with leaf angles in lower, middle and upper leaves all affected in similar ways[4]. For example, *liguleless1* (*lg1*) and *liguleless2* (*lg2*) have a crucial role in establishing the blade–sheath boundary and their null alleles have canopy-wide vertical leaves[13,14]. Candidate genes that control leaf angle at specific layers or throughout the canopy have been identified in sorghum[15,16]. However, genes that could differentially regulate leaf angles at different canopy layers to generate a smart-canopy-like plant architecture have so far not been identified in maize. Additionally, dense planting causes canopy shade and triggers shade-avoidance responses[17]. Substantial progress has been made in identifying the molecular mechanisms regulating shade-induced stem elongation in the model dicotyledonous plant *Arabidopsis thaliana*[17]. By contrast, how leaf angle—a major trait determining the canopy architecture of the world's most produced crop—is dynamically regulated as planting density increases remains largely unknown.

Identification of *lac1*

In a population of the maize inbred line W22, we identified a natural mutant exhibiting upright upper leaves, less erect middle leaves and relatively flat lower leaves (Fig. 1a). Compared with wild-type W22, this mutant showed varying degrees of reduction in leaf angles throughout the canopy, with the upper leaf angles having the greatest decrease, followed by the middle and lower leaf angles (Fig. 1b and Extended Data Fig. 1a). This leaf angle distribution across the plant conforms to the architecture characteristic proposed in the smart-canopy ideotype[5], we therefore named this mutant *leaf angle architecture of smart canopy 1* (*lac1*). As the ligular region is the key tissue that determines maize leaf angle[10,12], we performed scanning electron microscopy and histological analyses on *lac1* and wild-type W22 plants in this region. Compared with W22, *lac1* had a narrower ligular band, leading to reduced auricle size at maturity (Extended Data Fig. 1b–j). Sclerenchyma cells in the ligular region provide mechanical strength for the blade. Compared with wild-type W22, *lac1* plants contained more layers of sclerenchyma cells in the ligular region (Extended Data Fig. 1k,l). As a result, the leaf midrib of *lac1* exhibited greater mechanical strength than that of W22 (Extended Data Fig. 1m), contributing to smaller leaf angles in *lac1* plants.

To examine whether *lac1* could improve population-level photosynthesis under dense planting, we grew *lac1* and wild-type W22 at five different densities and measured photosynthetically active radiation at different canopy layers one week after pollination. *lac1* plants had greater light penetration to lower leaves than wild-type W22 across all planting densities (Fig. 1c,d). We measured net photosynthetic rates of ear leaves of *lac1* and W22 plants. Rates in ear leaves of W22 declined rapidly as planting density increased, however the ear leaves of *lac1* maintained relatively high net photosynthesis across these planting densities (Fig. 1e). Further characterization of photosynthetic parameters at a density of 120,000 plants per hectare showed that the ear leaves of *lac1* had improved diurnal changes, light-response curves and CO_2-response curves of net photosynthesis (Extended Data Fig. 1n–p). These results suggested that the canopy architecture in *lac1* improved light penetration and enhanced photosynthetic efficiency under dense canopies.

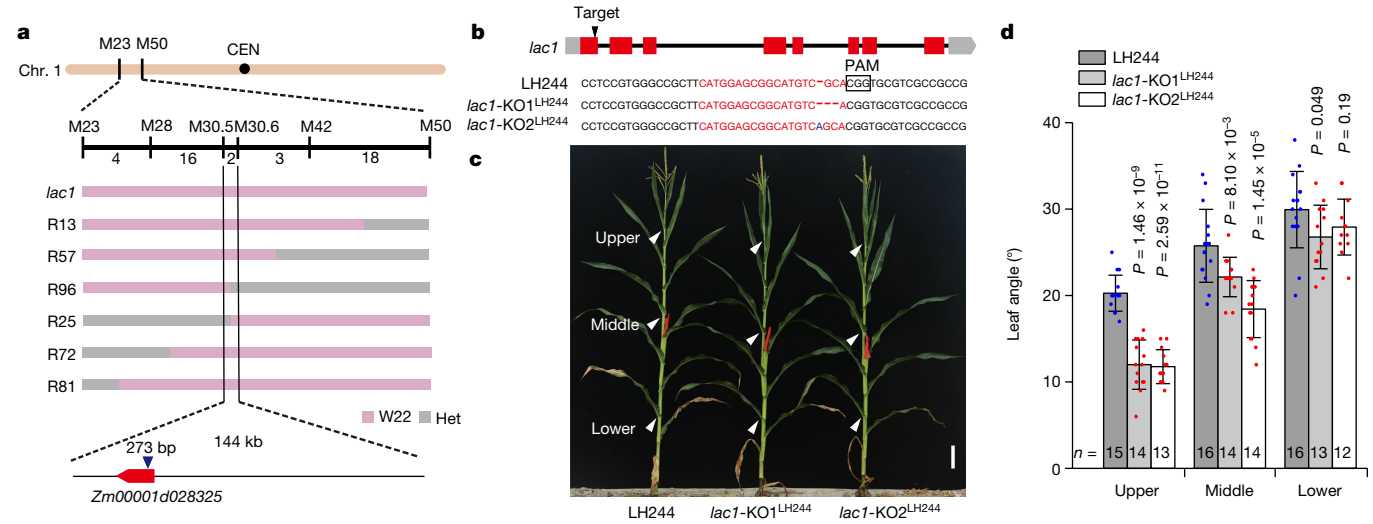

Fig. 2 | *DWF4* controls *lac1*. **a**, Positional cloning of *lac1*. *lac1* was delimited to a 144-kb physical region containing an annotated gene, *Zm00001d028325*, which encodes a homologue of rice and *Arabidopsis DWF4*. *lac1* contains a 273-bp insertion in the coding sequence of *DWF4* that causes a premature termination of the encoded protein. CEN, centromere; Chr., chromosome. The pink and grey segments indicate regions that are homozygous for W22 and heterozygous (het) regions, respectively. **b**, Two homozygous CRISPR–Cas9 knockout lines with deletions or insertions in the target site of *lac1*. A schematic of the gene and the wild-type sequence are shown at the top. The target site is highlighted in red, and the protospacer-adjacent motif (PAM) sequence is indicated by the black box. Dashed lines represent deletions. **c**, Plant phenotypes of *lac1*-knockout lines (*lac1*-KO1^{LH244} and *lac1*-KO2^{LH244}) and the wild type (LH244). White arrows indicate the lower, middle and upper leaves, from which leaf angle was scored. Scale bar, 18 cm. **d**, Comparison of the upper, middle and lower leaf angles between *lac1*-knockout lines (*lac1*-KO1^{LH244} and *lac1*-KO2^{LH244}) and LH244 grown at 82,500 plants per hectare. Data are mean ± s.d. *n* represents the number of biologically independent samples. In **d**, a two-tailed Student's *t*-test was used to determine *P* values.

Induction of the shade-avoidance response is a major factor that limits yield under dense planting. To examine the shade-avoidance response of *lac1*, we planted *lac1* and wild-type W22 in white light and simulated shade (low-red to far-red light ratio (low-red:far-red)). In white light, mesocotyl lengths for *lac1* and W22 were similar (Extended Data Fig. 1q,s). In simulated shade (low-red:far-red = 0.2), *lac1* mesocotyl lengths were significantly shorter than W22, indicating that the shade-avoidance response in *lac1* is attenuated (Extended Data Fig. 1r,t). In the same field used for measuring photosynthetic parameters, we also scored leaf angle, plant height, ear height and stem diameter. As planting density increased, ear height tended to increase, and leaf angle tended to decrease in both *lac1* and W22. However, the relative changes in *lac1* ear height and leaf angle with increasing planting densities were smaller than those of W22 (Fig. 1f–h and Extended Data Fig. 1u–w). These results suggest that *lac1* has attenuated shade-avoidance responses, which is an essential characteristic for realizing yield gains under dense planting.

lac1 is caused by mutation in *DWF4*

To determine the genetic basis of the *lac1* mutation, we crossed *lac1* with W22. In the resulting 112 F_2 progeny, 86 plants had architecture similar to W22 and 26 plants had *lac1*-like architecture, fitting a segregation ratio of 3:1 (χ^2 test, $P = 0.66$), indicating that *lac1* is controlled by a single recessive gene. To fine map *lac1*, we crossed *lac1* with the maize inbred line Mo17, which has large leaf angles throughout the canopy (Extended Data Fig. 2a,b). We planted an F_2 population containing 7,400 individuals, from which 200 plants were phenotyped for upper leaf angle and genotyped with genome-wide markers for linkage analysis. A bi-modal distribution in upper leaf angle was observed in this small F_2 population (Extended Data Fig. 2c,d) and linkage analysis located *lac1* on chromosome 1 (Supplementary Table 1). One hundred and fourteen extreme individuals displaying the typical *lac1*-like phenotype were identified from the F_2 population of *lac1* × Mo17 and used for fine mapping. *lac1* was delimited to a 144-kb physical region containing a single annotated gene, *Zm00001d028325*, which is predicted to encode a cytochrome P450 that catalyses C-22 hydroxylation—the rate-limiting step of brassinosteroid biosynthesis[18] (Fig. 2a). *lac1* is a homologue of *DWF4* in rice and *Arabidopsis*[19–21] (Extended Data Fig. 2e). Sequence comparison revealed that the *lac1* mutant contains a 273-bp transposon insertion in the second exon of *DWF4* that causes truncation of the protein product (Fig. 2a and Extended Data Fig. 2f).

To verify the function of *lac1*, we first constitutively overexpressed *lac1* under the control of the maize *Ubiquitin* promoter in the inbred line B104. The overexpression lines (*lac1*-OE1^{B104} and *lac1*-OE2^{B104}) had wider leaf angles in lower, middle and upper leaf layers relative to wild-type B104 (Extended Data Fig. 2g–i). We edited *lac1* using CRISPR–Cas9[22] in the inbred line LH244 and obtained two homozygous lines carrying frameshift mutations (*lac1*-KO1^{LH244} and *lac1*-KO2^{LH244}) (Fig. 2b). Both knockout lines show *lac1*-like phenotypes, with the upper leaf angles being reduced the most, followed by the middle and lower leaf angles compared with wild-type LH244 (Fig. 2c,d and Extended Data Fig. 3a). Similar to *lac1* plants, *lac1*-KO2^{LH244} plants had smaller auricles, more sclerenchyma layers in the ligular region, and stronger mechanical strength of leaf midribs relative to wild-type LH244 (Extended Data Fig. 3b–f). We planted *lac1*-KO2^{LH244} under five different densities to quantify photosynthetic capacity and shade-avoidance responses. Similar to the observations in *lac1*, *lac1*-KO2^{LH244} exhibited enhanced photosynthetic capacity and attenuated shade-avoidance responses (Extended Data Fig. 4a–l). To examine whether *lac1* affected brassinosteroid accumulation, we profiled brassinosteroids in the ligular region of *lac1*. Brassinolide was not detected in our samples but 6-deoxocastasterone and castasterone (the immediate precursor of brassinolide) were detected. *lac1* plants had less 6-deoxocastasterone and castasterone than wild-type W22 (Extended Data Fig. 3g,h). Collectively, these data suggest that *DWF4* controls *lac1* and that brassinosteroid biosynthesis is disturbed in *lac1* plants.

To further examine the role of *lac1* in regulating maize leaf angle architecture, we performed a cross-canopy *lac1* expression assay using 219 diverse maize inbred lines with contrasting leaf angle architecture. *lac1* expression in the upper ligular region is highly and positively correlated with upper leaf angle ($r = 0.36$, $P = 2.56 \times 10^{-6}$), and the correlations

between *lac1* expression in the middle and lower ligular regions and the middle and lower leaf angles decreased to much lower levels (r = 0.09 and 0.03 for middle and lower leaf angle, respectively) (Extended Data Fig. 5a). This population-level analysis further demonstrated that *lac1* exerts a stronger effect on upper leaf angles than on middle and lower leaf angles.

In contrast to the *Arabidopsis dwf4* mutant that has a severe dwarf phenotype[20,21], maize *lac1* null alleles have normal plant height, suggesting the presence of other functionally redundant genes. LAC1 shares 42% amino acid identity with Zm00001d003349, a cytochrome P450 with closest identity to rice D11 (Extended Data Fig. 2e). To examine the genetic relationship between *lac1* and *D11*, we knocked out *D11* in the LH244 genetic background (*D11*-KO1 and *D11*-KO2), then created double mutants for *lac1* and *D11* (Extended Data Fig. 5b,c). The single mutants of *D11* have a dwarf phenotype, whereas the *lac1* and *D11* double mutants show more severe phenotypes, including dwarfism, malformed leaves and aberrant inflorescences (Extended Data Fig. 5c). Furthermore, *D11* was up-regulated in *lac1*-knockout plants (Extended Data Fig. 5d). These results suggest that *D11* may function partially redundantly with *lac1* via a compensation mechanism that is frequently observed between paralogues[23]. *D11* may have a role in maintaining brassinosteroid levels for proper growth and development of the whole plant, whereas *lac1* may instead contribute specifically to maintenance of brassinosteroid levels for leaf inclination. Similarly, rice *D11* also functions redundantly with *DWF4*, mutations in which confer erect leaves with minor impacts on other important agronomic traits and improve rice yields under dense planting[19]. Manipulation of *DWF4* offers a promising approach to specifically tailor plant architecture for high-density planting.

RAVL1 directly activates *lac1* expression

We previously cloned two QTLs that regulate maize leaf angle and demonstrated that the B3 transcription factor RAVL1 functions as a crucial regulator of leaf angle[10]. RAVL1 directly activates the expression of *brd1*, which encodes a C-6 oxidase that catalyses the final steps of brassinosteroid biosynthesis, to promote brassinosteroid accumulation in the ligular region and thus increase leaf angle[10]. Here we tested whether RAVL1 could similarly regulate *lac1* and *D11*. *lac1* and *D11* were down-regulated in *RAVL1*-knockout plants, similar to *brd1* (Extended Data Fig. 5e,l). The putative RAVL1-binding elements E-box and CANNTG are present in the promoters of *lac1* and *D11* (Extended Data Fig. 5f,m). Yeast one-hybrid assays (Extended Data Fig. 5g,n), electrophoretic mobility shift assays (EMSAs) (Extended Data Fig. 5h,o), and chromatin immunoprecipitation (ChIP)–quantitative PCR analyses (Extended Data Fig. 5i,p) showed that RAVL1 could directly bind the *lac1* and *D11* promoters. Transient expression assays in maize protoplasts showed that RAVL1 could directly activate *lac1* and *D11* expression (Extended Data Fig. 5j,k,q,r). Combined with our previous results[10], we conclude that RAVL1 directly regulates the expression of these brassinosteroid biosynthesis genes to promote brassinosteroid accumulation in the ligular region, thus ultimately increasing leaf angle.

A phyA–RAVL1 module regulates *lac1*

Phytochromes are low-red and far-red light photoreceptors in plants that have a major role in mediating shade-avoidance responses[24,25]. The maize genome contains two *phyA* genes (*phyA1* and *phyA2*) and two *phyB* genes[26,27] (*phyB1* and *phyB2*). We tested whether RAVL1 is regulated by light by physical interactions with phyA and phyB proteins. We first performed split firefly luciferase complementation imaging assays in tobacco leaf cells. RAVL1 physically interacted only with phyA1 and phyA2 (Fig. 3a,b), but an interaction was not detected with phyB1 and phyB2 (Extended Data Fig. 6a,b). Interactions between RAVL1 and phyA proteins were confirmed by in vitro pull-down assays (Extended Data Fig. 6c–f). Phytochromes exist in vivo in two photo-convertible forms, Pr and Pfr, with Pfr being the biologically active form[24,25]. To determine which form(s) of phyA interact with RAVL1, we performed co-immunoprecipitation assays by transiently expressing RAVL1–MYC and phyA1–GFP or phyA2–GFP in tobacco leaves. Protein extracts were exposed to 5 min of far-red light alone, or 5 min of far-red light followed immediately by 5 min of red light. RAVL1 could interact with both Pfr and Pr forms of phyA1 and phyA2 (Fig. 3c).

To explore the role of *phyA1* and *phyA2* in regulating leaf angle, we used CRISPR–Cas9 to edit *phyA1* and *phyA2* in the LH244 background. We designed a conserved guide RNA (gRNA) that edits both *phyA1* and *phyA2*, and obtained two homozygous *phyA1 phyA2* double mutants carrying frameshift mutations in the two genes (*phyA*-KO1 and *phyA*-KO2) (Extended Data Fig. 6g,h). Compared with wild-type LH244, the double mutants had wider upper leaf angles, but had much smaller changes on middle and lower leaf angles than LH244 (Extended Data Fig. 6i), indicating that *phyA* genes mainly contribute to regulating leaf angles in the upper canopy.

To examine how *phyA* genes and *RAVL1* respond to shade, wild-type LH244 and *phyA1 phyA2* double mutant seedlings were grown in white light or simulated shade (low-red:far-red = 0.2) for two weeks, and leaves were sampled for immunoblotting using anti-phyA and anti-RAVL1 antibodies. In LH244 seedlings, phyA proteins were almost undetectable in white light, but accumulated to high levels in shade (Fig. 3d), whereas RAVL1 accumulated at lower levels in shade than in white light (Fig. 3d). However, in *phyA1 phyA2* double mutant seedlings, RAVL1 accumulated at similar levels in both white light and shade treatments (Fig. 3d). To further probe this regulation, wild-type LH244 and *phyA* double mutant seedlings were first grown under 16:8 h light:dark cycles for 2 weeks, and then transferred to continuous white light or simulated shade conditions for the indicated times ranging from 1 h to 12 h. Immunoblot analyses with LH244 seedlings revealed that, in white light, phyA levels were low, whereas RAVL1 remained at high levels (Fig. 3e,f). By contrast, in response to shade, phyA abundance in LH244 seedlings gradually accumulated to higher levels and RAVL1 gradually declined (Fig. 3e,f). However, in *phyA1 phyA2* double mutant seedlings, RAVL1 abundance remained largely unchanged under shade conditions (Fig. 3g,h). These results suggest that phyA proteins repress RAVL1 accumulation in the shade.

To further examine the regulatory relationship between phyA and RAVL1, we performed cell-free degradation assays using recombinant His–RAVL1 proteins and total protein extracts from wild-type LH244 and *phyA* double mutant seedlings grown in white light and shade conditions. Degradation of His–RAVL1 was much faster in total protein extracts from LH244 seedlings grown in the shade than in white-light conditions, whereas shade-induced degradation of RAVL1 was impaired in the *phyA* double mutant (Fig. 3i–l). However, the presence of MG132 (an inhibitor of the 26S proteasome) inhibited the reduction of RAVL1 proteins in the shade (Fig. 3i,k). Together, these data indicate that phyA proteins promote the degradation of RAVL1 in the shade via the 26S proteasome pathway.

To examine the effects of phyA–RAVL1 interactions on *lac1* expression, we performed transient expression assays in tobacco leaves. In shade, co-expression of phyA1–GFP or phyA2–GFP, together with RAVL1–MYC, significantly repressed RAVL1–MYC to activate *lac1* and *D11* promoters (Fig. 3m–o and Extended Data Fig. 6j,k). However, such inhibitory effects of phyA proteins were attenuated in white light (Fig. 4o and Extended Data Fig. 6k), possibly owing to the destabilization of phyA in white light. Consistent with these results, *lac1* was down-regulated in shade over white light (Extended Data Fig. 6l).

lac1 enhances yields at high densities

To evaluate the effect of *lac1* on yield under dense planting, we performed a series of field trials (Fig. 4 and Extended Data Fig. 7). We first

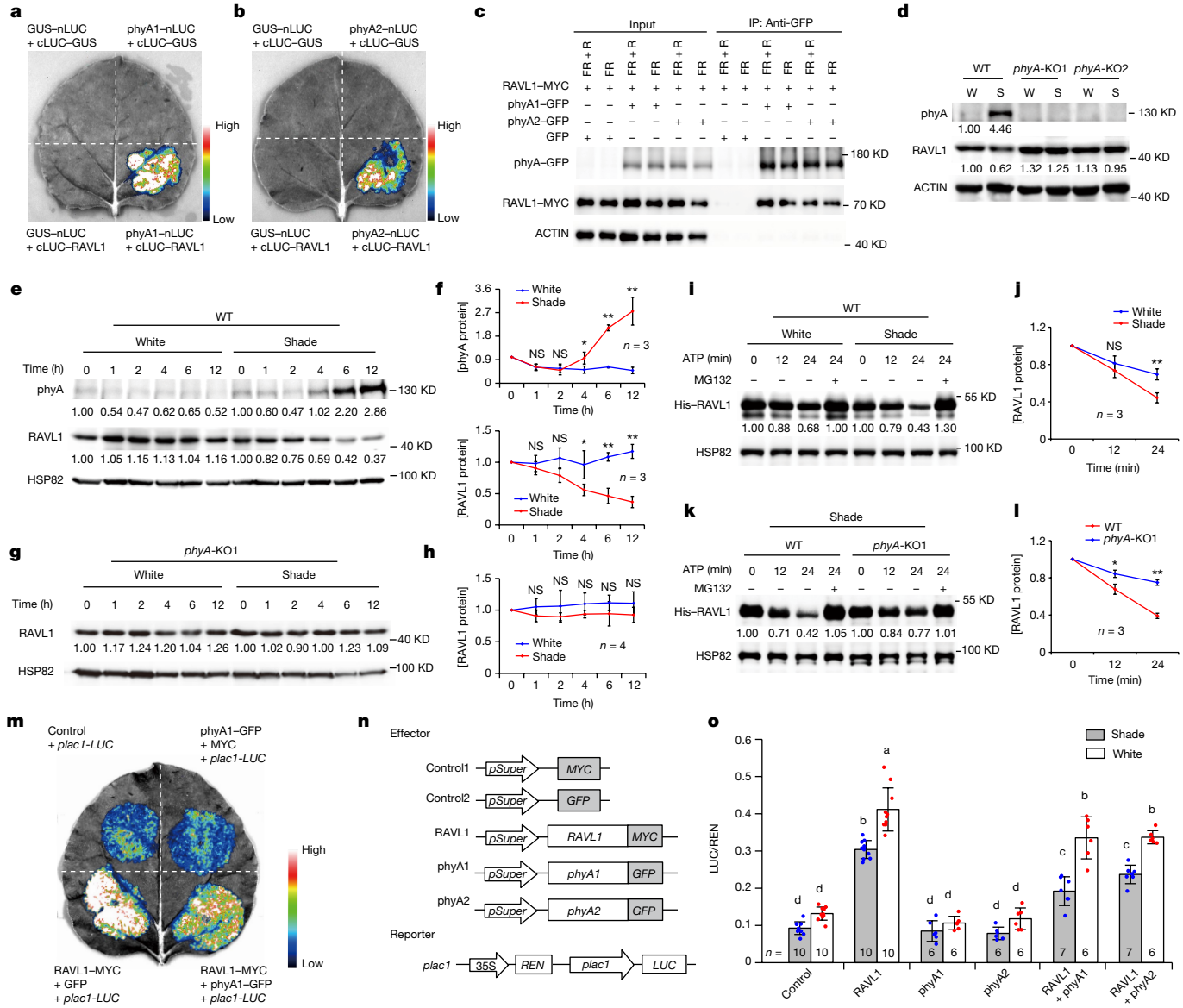

Fig. 3 | phyA–RAVL1-mediated light signalling regulates *lac1* expression. **a**,**b**, RAVL1 physically interacts with phyA1 (**a**) and phyA2 (**b**) in *Nicotiana benthamiana*. **c**, RAVL1 interacts with both Pfr and Pr forms of phyA1 and phyA2. IP, immunoprecipitation; R, red light; FR, far-red light. **d**, Immunoblot showing phyA and RAVL1 in two-week-old wild-type and *phyA*-knockout (*phyA*-KO1 and *phyA*-KO2) seedlings grown in white light (W) and simulated shade (S) conditions (low-red:far-red = 0.2). WT, wild type. **e**–**h**, phyA and RAVL1 abundance in two-week-old wild-type and *phyA*-KO1 seedlings transferred to white light or simulated shade for the indicated times. In **d**–**h**, phyA and RAVL1 proteins were detected with phyA antibody and RAVL1 antibody, respectively, and ACTIN and HSP82 served as loading controls. **i**–**l**, phyA proteins can induce the degradation of RAVL1 in shade. Immunoblots show the abundance of His–RAVL1 incubated with total proteins extracted from wild-type (**i**, quantified in **j**) and *phyA* mutant (**k**, quantified in **l**) seedlings with white light or shade in the presence of 2 mM ATP for the indicated times. RAVL1 was detected with an anti-His antibody. HSP82 served as a loading control. Band intensities were quantified with ImageJ. **m**, Effects of co-expressing RAVL1 and phyA1 on *lac1* expression in *N. benthamiana* grown in shade. **n**, Schematic representation of the effectors and reporter constructs used in the transient expression assays. **o**, phyA1 and phyA2 repress RAVL1 to activate the expression of *lac1* in shade. In **f**,**h**,**j**,**l**, data are mean ± s.d.; *n* represents numbers of independent experiments; two-tailed Student's *t*-test was used to determine *P* values. In **o**, data are mean ± s.d.; *n* represents numbers of biologically independent samples; different letters indicate statistically significant differences ($P < 0.05$, two-way ANOVA with Tukey's test). All experiments were repeated two to four times with similar results.

planted the *lac1* natural mutant and its wild type (W22) in Tieling (41.5° N, 123.2° E) and Sanya (18.2° N, 109.1° E), China in 2020 and 2021, with each trial containing five different planting densities and three biological replicates (Supplementary Fig. 1). Grain yield per plant of *lac1* and wild-type W22 decreased as planting density increased, however, the decline in *lac1* was lower (Fig. 4a and Extended Data Fig. 7a–j). As a result, *lac1* had higher grain yield than W22 controls under high planting densities (Fig. 4b and Extended Data Fig. 7a–j). We also conducted similar field trials for the *lac1*-knockout line *lac1*-KO2^{LH244} (Cas9-free) in Tongzhou (39.9° N, 116.4° E), China in 2022. Similar to the *lac1* natural mutant, *lac1*-KO2^{LH244} had higher yield than wild-type LH244 under high planting densities (Fig. 4c,d and Extended Data Fig. 7k,l).

To further evaluate the effect of *lac1* in a hybrid background, we created F_1 hybrids of *lac1* × *lac1*-KO2^{LH244} and of the wild-type combination (W22 × LH244). As expected, the F_1 hybrid of *lac1* × *lac1*-KO2^{LH244} displayed *lac1*-like phenotypic changes, with maximum reduction in the upper leaf angles and minimum reduction in the lower leaf angles compared with the F_1 hybrid of W22 × LH244 (Fig. 4e,f). We also measured

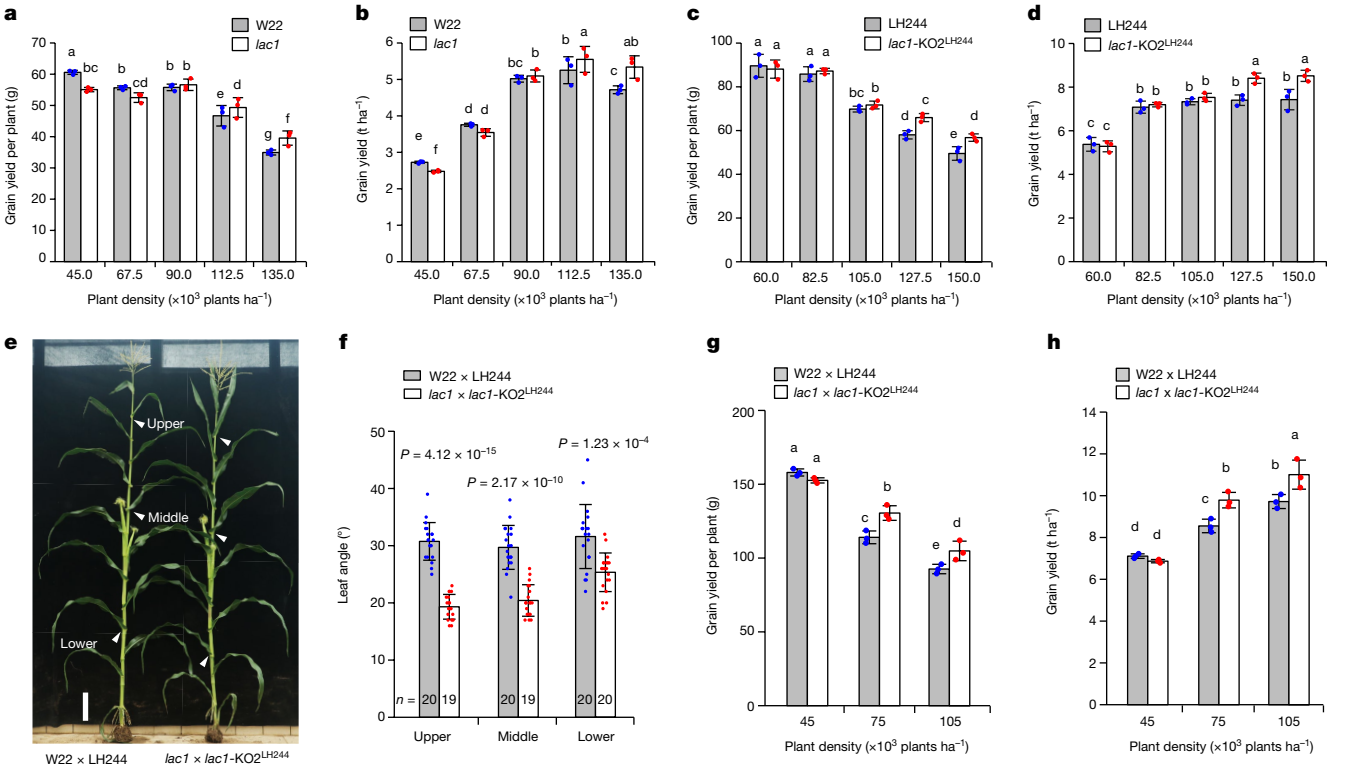

Fig. 4 | *lac1* enhances maize yields in inbreds and hybrids under high planting densities. a,**b**, Comparison of grain yield per plant (**a**) and grain yield per hectare (**b**) between *lac1* and wild-type W22 at indicated planting densities in a field trial in Tieling, China in 2020. **c**,**d**, Comparison of grain yield per plant (**c**) and grain yield per hectare (**d**) between *lac1*-KO2^{LH244} and wild-type LH244 at indicated planting densities in a field trial in Tongzhou, China in 2022. **e**,**f**, Comparison of plant phenotypes (**e**) and leaf angles in upper, middle and lower leaves (**f**) between the F_1 hybrid of *lac1* × *lac1*-KO2^{LH244} and the wild-type combination W22 × LH244 at a planting density of 75,000 plants per hectare. In **e**, white arrows indicate the lower, middle and upper leaves from which leaf angle was scored. Scale bar, 22 cm. **g**,**h**, Comparison of grain yield per plant (**g**) and grain yield per hectare (**h**) between the F_1 hybrid of *lac1* × *lac1*-KO2^{LH244} and the wild-type combination W22 × LH244 at indicated planting densities in a field trial in Shangzhuang, China in 2022. In **a**–**d**,**g**,**h**, data are mean ± s.d.; $n = 3$ biological replicates in a split-plot design); different letters indicate statistically significant differences ($P < 0.05$, PROC MIXED with Fisher's least significant difference test in SAS). In **f**, data are mean ± s.d.; *n* represents numbers of biologically independent samples; two-tailed Student's *t*-test was used to determine *P* values.

the shade-avoidance response and photosynthetic capacity of the F_1 hybrid of *lac1* × *lac1*-KO2^{LH244} under different planting densities. Similar to the observations in *lac1* and *lac1*-KO2^{LH244}, the F_1 hybrid of *lac1* × *lac1*-KO2^{LH244} had enhanced photosynthetic capacity and attenuated shade-avoidance responses in ear height and leaf angle at high densities, compared with the F_1 of W22 × LH244 (Extended Data Fig. 8a–l). We further scored the yields of the F_1 hybrids of *lac1* × *lac1*-KO2^{LH244} and of W22 × LH244 under different planting densities in two locations (Shangzhuang and Tongzhou, Beijing, China) in 2022. The F_1 hybrid of *lac1* × *lac1*-KO2^{LH244} had higher grain yield than that of W22 × LH244 under high densities in both locations (Fig. 4g,h and Extended Data Fig. 7m–r). Collectively, these data demonstrate that *lac1* enhances yield of both inbred and hybrid lines under high-density planting conditions.

We previously showed that the teosinte allele at *RAVL1* confers upright leaf angle and enhances grain yield under high-density planting[10]. To compare the yield potential of *lac1* and *RAVL1*, we crossed the *lac1* natural mutant (*lac1*^{mutant}) with the teosinte near-isogenic line (NIL) for *RAVL1* (*RAVL1*^{teosinte}). The genetic background of both *lac1*^{mutant} and *RAVL1*^{teosinte} is W22. From the derived F_2 population, we isolated four types of homozygous genotype combinations: *lac1*^{W22} *RAVL1*^{W22}, *lac1*^{W22} *RAVL1*^{teosinte}, *lac1*^{mutant} *RAVL1*^{W22} and *lac1*^{mutant} *RAVL1*^{teosinte} (Extended Data Fig. 9a). These four genotypes were planted under three planting densities (90,000, 120,000 and 150,000 plants per hectare) with three biological replicates in Tongzhou and Sanya in 2023. At both locations, under the density of 90,000 plants per hectare, the four genotypes all had similar grain yields (Extended Data Fig. 9b,c). However, under the highest density of 150,000 plants per hectare, *lac1*^{mutant} *RAVL1*^{W22} had higher grain yield than *lac1*^{W22} *RAVL1*^{teosinte} (Extended Data Fig. 9b,c), indicating the advantage of smart-canopy-like plant architecture over canopy-wide upright plant architecture at this density. Notably, *lac1*^{mutant} *RAVL1*^{teosinte} out-yielded both *lac1*^{mutant} *RAVL1*^{W22} and *lac1*^{W22} *RAVL1*^{teosinte} at the density of 150,000 plants per hectare (Extended Data Fig. 9b,c), suggesting that pyramiding two elite alleles at *lac1* and *RAVL1* could synergistically boost maize yields under high-density planting.

Creating a smart-canopy using HI-Edit

Gene editing is changing plant breeding techniques[22]. Doubled haploid technology is broadly used to rapidly produce homozygous plants for accelerating crop breeding, especially in maize[22]. Two novel breeding technologies that combine haploid-induction and gene-editing technology—haploid-inducer editing (HI-Edit) and haploid-inducer-mediated genome editing (IMGE)—enable gene editing directly in commercial varieties[28,29]. However, owing to constraints in genetic transformation, applications of these two methods currently require initial delivery of the gene-editing cassette into a transgene recipient that has a high transformation efficiency. The transgene recipient carrying the gene-editing cassette is then crossed and backcrossed with a haploid inducer to introgress the editing machinery into the haploid-inducer genome for subsequent haploid-induction editing. This two-step process usually takes several generations and is also likely to impair the haploid-induction rate owing to incomplete

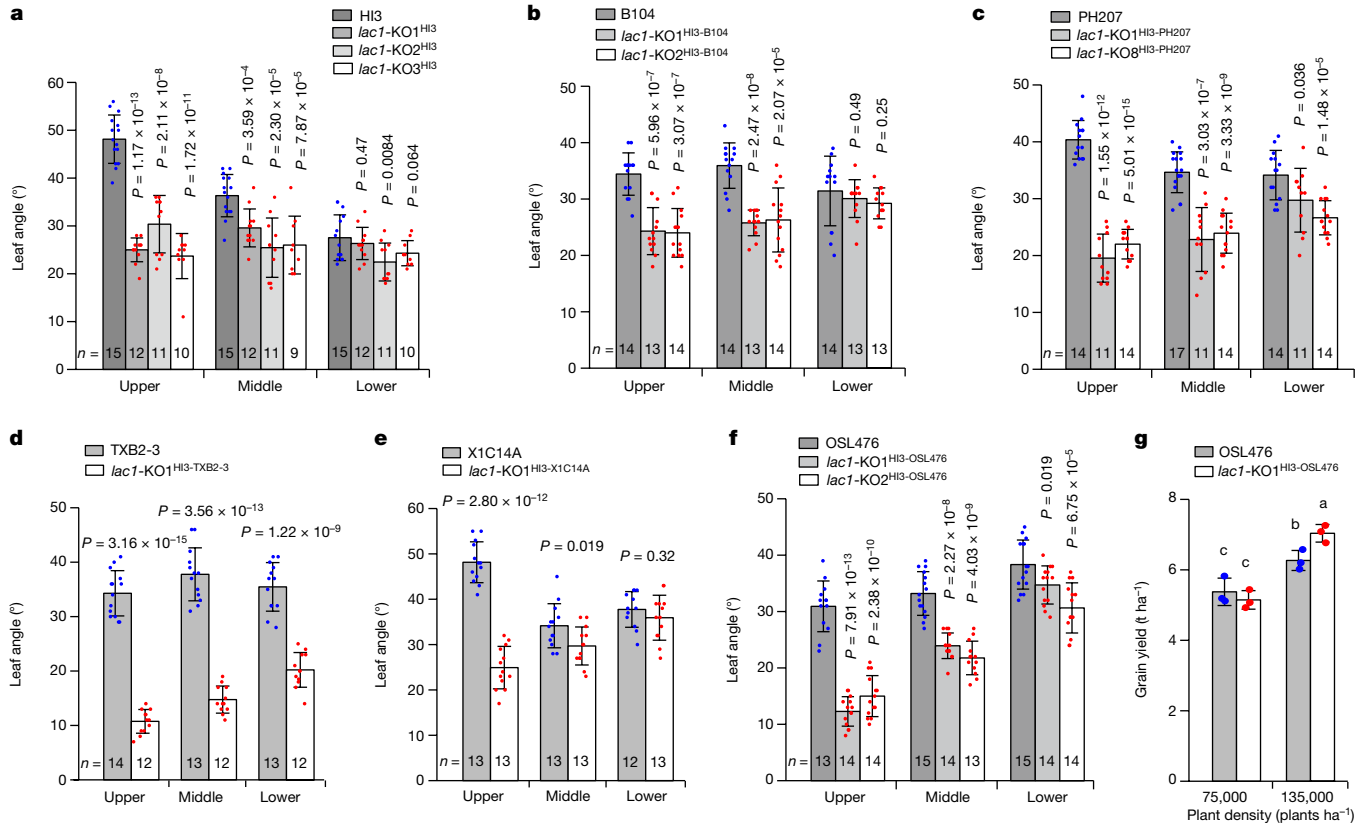

Fig. 5 | Creating optimal plant architecture for a smart canopy using haploid-induction editing. a, Comparison of leaf angles in upper, middle and lower leaves between the edited haploid-inducer lines (*lac1*-KO1^{HI3}, *lac1*-KO2^{HI3} and *lac1*-KO3^{HI3}) and the original haploid-inducer line (HI3). **b**, Comparison of leaf angles in upper, middle and lower leaves between B104 and the edited doubled haploids from B104 (*lac1*-KO1$^{HI3\text{-}B104}$ and *lac1*-KO2$^{HI3\text{-}B104}$). **c**, Comparison of leaf angles in upper, middle and lower leaves between PH207 and the edited doubled haploids from PH207 (*lac1*-KO1$^{HI3\text{-}PH207}$ and *lac1*-KO8$^{HI3\text{-}PH207}$). **d**, Comparison leaf angles in upper, middle and lower leaves between OSL476 and the edited doubled haploids from OSL476 (*lac1*-KO1$^{HI3\text{-}OSL476}$ and *lac1*-KO2$^{HI3\text{-}OSL476}$). **e**, Comparison of angles in upper, middle and lower leaves between TXB2-3 and the edited doubled haploid from TXB2-3 (*lac1*-KO1$^{HI3\text{-}TXB2\text{-}3}$). **f**, Comparison of leaf angles in upper, middle and lower leaves between X1C14A and the edited doubled haploid from X1C14A (*lac1*-KO1$^{HI3\text{-}X1C14A}$). Measurements in **a**–**f** were performed at a planting density of 82,500 plants per hectare. **g**, Field trials for OSL476 and the edited doubled haploids (*lac1*-KO1$^{HI3\text{-}OSL476}$) conducted in Sanya in 2023. In **a**–**f**, data are mean ± s.d.; *n* represents numbers of biologically independent samples; two-tailed Student's *t*-test was used to determine *P* values. In **g**, data are mean ± s.d.; *n* = 3 biological replicates in a split-plot design; different letters indicate statistically significant differences ($P < 0.05$, PROC MIXED with Fisher's least significant difference test in SAS).

recovery of the haploid-inducer background. The most efficient strategy would therefore be to directly use haploid-inducer lines for genetic transformation.

To this end, we optimized an *Agrobacterium*-mediated transformation protocol and successfully performed genetic transformation for a haploid-inducer line, HI3 (Extended Data Fig. 10a–n). We introduced the CRISPR–Cas9 cassette targeting *lac1* into HI3. We obtained three Cas9-positive lines carrying homozygous frameshift mutations in *lac1* (*lac1*-KO1^{HI3}, *lac1*-KO2^{HI3} and *lac1*-KO3^{HI3}) (Extended Data Fig. 11a–c). *lac1*-KO1^{HI3}, *lac1*-KO2^{HI3} and *lac1*-KO3^{HI3} all exhibit *lac1*-like phenotypic changes compared with HI3 controls (Fig. 5a). We collected their pollen to pollinate 43 maize inbred lines that have conserved sequences at the *lac1* CRISPR–Cas9 target site (Extended Data Fig. 10p and Supplementary Table 2). From the resulting F_1 seeds, putative haploid seeds (D_0 seeds) with a colourless scutellum and a pigmented aleurone were identified[30], which were then germinated and treated with colchicine to promote chromosome doubling. D_0 seedlings were then planted in the field and genotyped to determine whether they lacked the *Cas9* transgene and the inducer allele *matl*[31–33] (Supplementary Fig. 2), which are only present in HI3. We sampled and sequenced 1,175 D_0 plants to identify potential edits in *lac1*. Eighty D_0 plants from 20 inbred lines carried homozygous mutations in *lac1*, giving an average haploid editing rate of 6.8% across the inbred lines (Supplementary Table 2 and Supplementary Fig. 3). D_0 plants carrying homozygous *lac1* mutations were selfed to obtain D_1 seeds, and D_1 seeds from five inbred lines (B104, PH207, OSL476, TXB2-3 and X1C14A) were planted in the field and scored for upper, middle and upper leaf angle (Extended Data Fig. 11a,b). The edited D_1 plants from the five inbred lines all presented *lac1*-like phenotypes, with the upper leaf angles having the greatest reduction (Fig. 5b–f and Extended Data Fig. 11d–h), indicating that they all acquired smart-canopy-like plant architecture. To further test the yield potential of the edited lines, we planted OSL476 and its edited doubled haploids under 2 planting densities (75,000 and 135,000 plants per hectare) with 3 biological replicates in Sanya in 2023. The edited and original OSL476 had similar yields at 75,000 plants per hectare. However, *lac1*-edited OSL476 significantly out-yielded the original OSL476 at a density of 135,000 plants per hectare (Fig. 5g).

Discussion

Developing high-density-tolerant cultivars is a major target in contemporary maize breeding. Here we report the identification of a natural mutant *lac1* that possesses both morphological and physiological adaptations to dense planting. First, in terms of morphology, *lac1* exhibits desirable smart-canopy-like leaf angle architecture, with upright upper leaves, less erect middle leaves and relatively flat lower leaves. These characters were associated with improved light harvesting and enhanced canopy photosynthesis under dense canopies. Second, in

terms of physiology, *lac1* has attenuated shade-avoidance responses. Shade-avoidance responses are adaptive changes that help individuals to outcompete their neighbours, but might affect reproductive yield under dense planting owing to reduced photoassimilate partitioning to grains, increased risk of lodging, precocious maturation and increased susceptibility to pests and diseases[17,25]. Attenuated shade-avoidance responses were selected during domestication and breeding for maize cultivars adapted to dense planting[34]. Field trials at four locations over four years robustly demonstrated that *lac1* could enhance maize yields in both inbred and hybrid lines under high planting densities. Furthermore, we found that *lac1* out-yielded the teosinte NIL of *RAVL1*, potentially hinting at the advantage of smart-canopy-like plant architecture over canopy-wide upright plant architecture under high-density conditions. Notably, pyramiding the two elite alleles at *lac1* and *RAVL1* synergistically further boosted maize yields under high-density planting. Our *lac1* field trials meet the criteria for assessing the effects of genes on crop yields proposed by Khaipho-Burch et al.[35]. Although further testing in additional commercial varieties is desirable, our findings demonstrate the potential of *lac1* serving as a genetic chassis for architectural engineering of a smart canopy for high-density cultivation in maize.

Obtaining a desired smart-canopy-like plant architecture requires manipulation of leaf angles specifically in the upper canopy. We analysed the effects of *lac1* in eight different maize inbred lines. Despite their distinct plant architectures, mutation of *lac1* consistently resulted in the strongest reduction in upper leaf angles, suggesting that *lac1* predominantly regulates upper leaf angle. We further performed a cross-canopy *lac1* expression assay in 219 inbred lines to evaluate its relative contribution to leaf angle variation across the plant. *lac1* expression has the highest correlation with upper leaf angle. This population-level analysis further indicates that *lac1* has a major role in specifically regulating upper leaf angle, explaining why loss of *lac1* in different genetic backgrounds would endow smart-canopy-like plant architecture.

Leaf angle is a shade-avoidance trait, and we found that upper leaf angle decreases as planting density increases. We propose a model to explain how *phyA*-mediated shade signalling modulates *lac1* expression to dynamically regulate upper leaf angle as planting density increases (Extended Data Fig. 12). At high planting densities, neighbour proximity induces a low low-red:far-red ratio perceived by leaves in the upper canopy. phyA photoreceptors accumulate and physically interact with the transcription factor RAVL1 to promote its degradation via the 26S proteasome pathway, thus inhibiting RAVL1-mediated *lac1* expression. This consequently reduces brassinosteroid accumulation in the ligular region and ultimately decreases upper leaf angles at high planting densities. In *lac1* mutants, phyA–RAVL1-mediated signalling is blocked, leading to attenuated shade-avoidance responses that contribute to retaining more resources that then boost seed yield under dense planting conditions.

Maize shows wide natural variation in leaf angle architecture (Supplementary Fig. 4). QTL mapping in maize[36] and genome-wide association study in sorghum[16] showed that the genetic mechanisms underlying leaf angle variation across the plant are complex and involve the coordinated regulation of genes controlling both canopy-wide and layer-specific leaf angles. Owing to heterogeneous light distribution in dense vegetation, leaves at different canopy layers are elicited by different shade signals[37,38], leading to leaf angles at each canopy layer are subject to different genetic regulation. Our study demonstrated that *lac1* predominantly regulates upper leaf angle, and the *phyA–RAVL1–lac1* module contributes to shade-induced decreases in upper leaf angle as planting density increases. How leaf angles in the middle and lower leaves are regulated and respond dynamically to planting density requires further work. It will be intriguing to investigate how canopy-wide and layer-specific leaf angle genes act coordinately to control leaf inclination at different canopy layers. Additional effort should be focused on further understanding how photoreceptors including phytochromes (*phyA* and *phyB*), cryptochromes (*cry1* and *cry2*) and the UV-B receptor UVR8[17,25] coordinate various plant hormone pathways to dynamically regulate leaf angle at different canopy levels in response to dense planting.

Rapidly introducing favourable alleles or edits identified from basic research into commercial varieties has long been a challenge. The conventional strategy involves repeated backcrossing introgression, but this is time consuming, laborious, and is sometimes affected by linkage drag. Haploid-induction editing technology (Hi-Edit and IMGE) can overcome these issues[28,29]. However, current applications still require a transgene recipient with a high transformation efficiency to facilitate transfer of the gene-editing machinery into the haploid inducer. Here we greatly simplified this process by successfully performing genetic transformation of the haploid-inducer line HI3. We crossed HI3 carrying the gene-editing cassette targeting *lac1* with 43 maize inbred lines to induce haploids. Homozygous *lac1* edits were identified in 20 inbred lines, and phenotypic analysis of edited D_1 plants from 5 inbred lines indicated that they all acquired smart-canopy-like plant architecture. Further optimization is necessary to increase the efficiency of genetic transformation and haploid-induction editing, potentially by using the morphogenetic regulators *Baby boom* and *Wuschel* to improve transformation[39] and using gamete-specific promoters to increase Cas9 activity during fertilization[28]. Using haploid inducers for genetic transformation and induction editing enables functional validation and breeding potential evaluation of genes of interest to be performed directly in elite commercial germplasm, bypassing the need for an intermediate transgene recipient to test gene function and then transfer the favourable allele to breeding germplasm. This strategy helps to close the gap between basic research and breeding applications and thus accelerates crop breeding.

Online content

Any methods, additional references, Nature Portfolio reporting summaries, source data, extended data, supplementary information, acknowledgements, peer review information; details of author contributions and competing interests; and statements of data and code availability are available at https://doi.org/10.1038/s41586-024-07669-6.

1. Assefa, Y. et al. Analysis of long term study indicates both agronomic optimal plant density and increase maize yield per plant contributed to yield gain. *Sci Rep.* **8**, 4937–4948 (2018).
2. Tian, F. et al. Genome-wide association study of leaf architecture in the maize nested association mapping population. *Nat. Genet.* **43**, 159–162 (2011).
3. Duvick, D. N. Genetic progress in yield of United States maize (*Zea mays* L.). *Maydica* **50**, 193–202 (2005).
4. Mantilla-Perez, M. B. & Maria, S. F. Differential manipulation of leaf angle throughout the canopy: current status and prospects. *J. Exp. Bot.* **68**, 5699–5717 (2017).
5. Ort, D. R. et al. Redesigning photosynthesis to sustainably meet global food and bioenergy demand. *Proc. Natl Acad. Sci. USA* **112**, 8529–8536 (2015).
6. Zhu, X. G., Long, S. P. & Ort, D. R. Improving photosynthetic efficiency for greater yield. *Annu. Rev. Plant. Biol.* **61**, 235–261 (2010).
7. van Dijk, M., Morley, T., Rau, M. L. & Saghai, Y. A meta-analysis of projected global food demand and population at risk of hunger for the period 2010-2050. *Nat. Food* **2**, 494–501 (2021).
8. Ray, D. K., Mueller, N. D., West, P. C. & Foley, J. A. Yield trends are insufficient to double global crop production by 2050. *PLoS ONE* **8**, e66428 (2013).
9. Qian, C. R. et al. Response of grain yield to plant density and nitrogen rate in spring maize hybrids released from 1970 to 2010 in Northeast China. *Crop J.* **4**, 459–467 (2016).
10. Tian, J. G. et al. Teosinte ligule allele narrows plant architecture and enhances high-density maize yields. *Science* **365**, 658–664 (2019).
11. Wang, B. et al. Genome-wide selection and genetic improvement during modern maize breeding. *Nat. Genet.* **52**, 565–571 (2020).
12. Cao, Y., Zhong, Z., Wang, H. & Shen, R. Leaf angle: a target of genetic improvement in cereal crops tailored for high-density planting. *Plant Biotechnol. J.* **20**, 426–436 (2022).
13. Walsh, J., Waters, C. A. & Freeling, M. The maize gene *liguleless2* encodes a basic leucine zipper protein involved in the establishment of the leaf blade-sheath boundary. *Genes Dev.* **12**, 208–218 (1998).
14. Moreno, M. A., Harper, L. C., Krueger, R. W., Dellaporta, S. L. & Freeling, M. *liguleless1* encodes a nuclear-localized protein required for induction of ligules and auricles during maize leaf organogenesis. *Genes Dev.* **11**, 616–628 (1997).

15. Natukunda, M. I., Mantilla-Perez, M. B., Graham, M. A., Liu, P. & Salas-Fernandez, M. G. Dissection of canopy layer-specific genetic control of leaf angle in Sorghum bicolor by RNA sequencing. *BMC Genomics* **23**, 14 (2022).
16. Mantilla-Perez, M. B., Bao, Y., Tang, L., Schnable, P. S. & Salas-Fernandez, M. G. Toward "smart canopy" sorghum: discovery of the genetic control of leaf angle across layers. *Plant Physiol.* **184**, 1927–1940 (2020).
17. Fernández-Milmanda, G. L. & Ballaré, C. L. Shade avoidance: expanding the color and hormone palette. *Trends Plant Sci.* **26**, 509–523 (2021).
18. Zhao, B. & Li, J. Regulation of brassinosteroid biosynthesis and inactivation. *J. Integr. Plant Biol.* **54**, 746–759 (2012).
19. Sakamoto, T. et al. Erect leaves caused by brassinosteroid deficiency increase biomass production and grain yield in rice. *Nat. Biotechnol.* **24**, 105–109 (2006).
20. Azpiroz, R., Wu, Y., LoCascio, J. C. & Feldmann, K. A. An *Arabidopsis* brassinosteroid-dependent mutant is blocked in cell elongation. *Plant Cell* **10**, 219–230 (1998).
21. Choe, S. et al. The DWF4 gene of *Arabidopsis* encodes a cytochrome P450 that mediates multiple 22 alpha-hydroxylation steps in brassinosteroid biosynthesis. *Plant Cell* **10**, 231–243 (1998).
22. Gao, C. X. Genome engineering for crop improvement and future agriculture. *Cell* **184**, 1621–1635 (2021).
23. Iohannes, S. D. & Jackson, D. Tackling redundancy: genetic mechanisms underlying paralog compensation in plants. *New Phytol.* **240**, 1381–1389 (2023).
24. Legris, M., Ince, Y. & Fankhauser, C. Molecular mechanisms underlying phytochrome-controlled morphogenesis in plants. *Nat. Commun.* **10**, 5219 (2019).
25. Casal, J. J. Photoreceptor signaling networks in plant responses to shade. *Annu. Rev. Plant Biol.* **64**, 403–427 (2013).
26. Sheehan, M. J., Kennedy, L. M., Costich, D. E. & Brutnell, T. P. Subfunctionalization of *PhyB1* and *PhyB2* in the control of seedling and mature plant traits in maize. *Plant J.* **49**, 338–353 (2007).
27. Sheehan, M. J., Farmer, P. R. & Brutnell, T. P. Structure and expression of maize phytochrome family homeologs. *Genetics* **167**, 1395–1405 (2004).
28. Kelliher, T. et al. One-step genome editing of elite crop germplasm during haploid induction. *Nat. Biotechnol.* **37**, 287–292 (2019).
29. Wang, B. B. et al. Development of a haploid-inducer mediated genome editing system for accelerating maize breeding. *Mol. Plant.* **12**, 597–602 (2019).
30. Meng, D. X., Liu, C. X., Chen, S. J. & Jin, W. W. Haploid induction and its application in maize breeding. *Mol. Breed.* **41**, 9 (2021).
31. Kelliher, T. et al. MATRILINEAL, a sperm-specific phospholipase, triggers maize haploid induction. *Nature* **542**, 105–109 (2017).
32. Liu, C. X. et al. A 4-bp insertion at *ZmPLA1* encoding a putative phospholipase a generates haploid induction in maize. *Mol. Plant.* **10**, 520–522 (2017).
33. Gilles, L. M. et al. Loss of pollen-specific phospholipase NOT LIKE DAD triggers gynogenesis in maize. *EMBO J.* **36**, 707–717 (2017).
34. Kebrom, T. H. & Brutnell, T. P. The molecular analysis of the shade avoidance syndrome in the grasses has begun. *J. Exp. Bot.* **58**, 3079–3089 (2007).
35. Khaipho-Burch, M. et al. Genetic modification can improve crop yields - but stop overselling it. *Nature* **621**, 470–473 (2023).
36. Tang, D. et al. Identification of QTL for leaf angle at canopy-wide levels in maize. *Euphytica* **217**, 75–91 (2021).
37. Huber, M., Nieuwendijk, N. M., Pantazopoulou, C. K. & Pierik, R. Light signalling shapes plant-plant interactions in dense canopies. *Plant Cell Environ.* **44**, 1014–1029 (2021).
38. Fiorucci, A. S. & Fankhauser, C. Plant strategies for enhancing access to sunlight. *Curr. Biol.* **27**, R931–R940 (2017).
39. Lowe, K. et al. Morphogenic regulators *Baby boom* and *Wuschel* improve monocot transformation. *Plant Cell* **28**, 1998–2015 (2016).

Methods

Plant materials

The natural mutant *lac1* was initially discovered in a population of maize inbred line W22 genetic background in the summer field of Tieling, China in 2018. To examine the genetic basis of *lac1*, we crossed *lac1* plants with the wild-type W22 in the winter field of Hainan, China in 2018. The generated F_1 seeds were then planted and selfed to produce F_2 seeds in Tieling in 2019. A total of 112 F_2 plants were planted for phenotypic analysis in Hainan in 2019. To fine map *lac1*, we crossed *lac1* plants with the inbred line Mo17 with canopy-wide large leaf angle, and the generated F_2 population was planted in Tieling in 2020 (Extended Data Fig. 2a–d). Knockout lines for *lac1* (*lac1*-KO1^{LH244} and *lac1*-KO2^{LH244}), *D11* (*D11*-KO1 and *D11*-KO1) and the double mutants for *phyA1* and *phyA2* (*phyA*-KO1 and *phyA*-KO2) were generated in the LH244 background. Double mutants for *lac1* and D11 were obtained from crosses between the single mutants *lac1*-KO2^{LH244}, *D11*-KO1 and *D11*-KO2. The *lac1* overexpression lines were generated in the B104 background. A total of 43 maize inbred lines having conserved sequence at the *lac1* target site were used for haploid-induction editing (Supplementary Table 2).

Positional cloning of *lac1*

An F_2 population containing 7,400 individuals from the *lac1* × Mo17 cross was planted. To determine the chromosomal location of *lac1*, 200 F_2 individuals were first phenotyped for upper leaf angle and genotyped with genome-wide markers for linkage analysis. A total of 20 molecular markers across the 10 maize chromosomes, 2 markers for each chromosome, were used in the linkage analysis (Supplementary Table 3). For each chromosome, the difference in upper leaf angle between the two homozygous genotypic classes at the two markers was tested with Student's *t*-test (Supplementary Table 1). This linkage analysis located *lac1* on chromosome 1. Accurately identifying homozygous recessive individuals from segregating population is a key step of fine mapping. We simultaneously planted a reference F_2 population containing 218 plants derived from the cross between W22 and Mo17 and analysed its distribution in upper leaf angle (Extended Data Fig. 2c). Based on the phenotypic distributions, a total of 114 extreme individuals exhibiting typical *lac1*-like phenotype were identified from the F_2 population of *lac1* × Mo17 for fine mapping *lac1*. Six molecular markers were progressively developed to determine the recombination breakpoints of the recessive individuals (Supplementary Table 3). Out of the 114 recessive individuals, 43 recombinants were found to carry recombination between markers M23 and M50. *lac1* was finally narrowed down to a 144-kb physical interval between markers M30.5 and M30.6 containing a single annotated gene based on the B73 reference genome (https://www.maizegdb.org). The discovery and positional cloning processes for *lac1* are summarized in Supplementary Fig. 5.

Leaf angle phenotyping, scanning electron microscopy and histological analysis

Leaf angle was measured as the angle between the stalk and the midrib of leaf blade using a protractor. The upper, middle and lower leaf angle represent the leaf angle of the first leaf below the flag leaf, the first leaf above the primary ear and the second leaf below the primary ear, respectively. Scanning electron microscopy analysis was performed as previously described[10]. Mutant *lac1* and wild-type W22 were planted in field. The ligular regions of mature and immature leaves at V3 stage were sampled and fixed immediately with 2.5% (v/v) glutaraldehyde in phosphate buffer (pH 7.0) for 6–7 h at 4 °C. The fixed samples were then dehydrated using a series of ethanol gradient from 30% to 100% (v/v) for 30 min at each step. After drying, the samples were coated with gold-palladium for 60 s and then observed under scanning electron microscope (Hitachi S-4700) using a 2-kV accelerating voltage. The length and width of cells in the ligular region were measured using the ImageJ software. The histological analysis was performed as previously described[10]. The ligular regions of mature leaves at V3, V9 and V13 stages were collected and fixed in the 3.7% (v/v) formaldehyde–acetic acid–alcohol solution (3.7% formaldehyde, 5% acetic acid and 50% ethanol). After shaking overnight, the samples were dehydrated and stained with fuchsine using a series of ethanol gradient from 50% to 100% (v/v). The dehydrated samples were soaked in HistoChoice Clearing Agent (Sigma) overnight and then embedded using paraffin (Leica), which were cut into 10-μm sections with a rotary microtome (Leica). The sections were observed and photographed using the ToupView software under a light microscope (Olympus CX23). The numbers of the abaxial and adaxial sclerenchyma cell layers were counted. To examine the mechanical strength of the leaf midrib of the upper, middle and lower leaves, the force that breaks the leaf midrib was measured with a digital force/length tester (WDF-50; WD).

RNA extraction and expression analysis

To examine how shade regulates *lac1* expression, wild-type (W22) seedlings were planted in white light and simulated shade (low-red:far-red = 0.2) for two weeks and then sampled to assay *lac1* expression. To investigate whether *lac1* and *D11* are regulated by *RAVL1*, the ligular regions of *RAVL1*-KO1 plants were sampled to assay the expression levels of *lac1* and *D11*. Total RNAs were extracted from frozen collected tissues using TRIzol (TIANGEN) and purified using an RNAclean Kit (TIANGEN) following the manufacturer's instructions. The purified total RNAs (1 μg) were then reverse transcribed with random primers and oligo(dT)$_{12–18}$ primers using StarScript II RT Mix with gDNA Remover (GenStar). Quantitative PCR was performed with qPCR Mix (GenStar) on an ABI 7500 real-time detection system (Applied Biosystems). Each expression assay contained three independent biological replicates. *Tubulin1* was used as the reference gene for normalization. The relative expression levels of target gene were quantified according to the comparative CT ($2^{-\Delta CT}$) method[40]. Primer sequences used in expression analyses are listed in Supplementary Table 4.

Cross-canopy *lac1* expression assay

A set of 219 inbred lines randomly selected from a maize association panel[41] were planted in the winter nursery in Sanya, China in 2023. The developing ligular regions of the lower (the second leaf below the primary ear), middle (the first leaf above the primary leaf) and upper (the second leaf below the flag leaf) leaves were sampled and *lac1* expression levels were profiled with *UBCP* as the reference gene. At maturity, the lower, middle and upper leaf angles were phenotyped. Pearson's correlation coefficients between leaf-specific *lac1* expression levels and corresponding leaf angles were calculated using R.

Genetic transformation

To generate the overexpression construct, the full-length coding sequence of *lac1* was amplified from B73 cDNA and cloned into pCAMBIA3300-GFP driven by the maize *Ubiquitin* promoter (*Ubi*), forming *Ubi*$_{pro}$*:lac1* fusion vector. For the CRISPR–Cas9 knockout vectors, the target sequences for *lac1*, *D11* and *phyA* genes were designed using CRISPR–P2.0 (http://crispr.hzau.edu.cn/CRISPR2/). To generate a double mutant for *phyA1* and *phyA2*, a conserved gRNA that could edit both *phyA1* and *phyA2* was designed. The target sequence was cloned into the pBUE411 vector under the control of the maize *Ubiquitin 1* promoter. All resulting vectors were transformed into *Agrobacterium tumefaciens* strain EHA105. *Agrobacterium*-mediated transformation using maize immature embryos was performed to generate transgenic plants[42–44]. The *Ubi*$_{pro}$*:lac1* fusion vectors were transformed to the maize inbred line B104. The CRISPR–Cas9 knockout constructs were transformed to the maize inbred line LH244. For genetic transformation of haploid-inducer lines, six different haploid-inducer lines were initially tested for embryonic callus induction ability using routine *Agrobacterium*-mediated maize genetic transformation methods[42–44]. We found that only one haploid line, HI3, produced suitable type-II embryogenic callus

(Extended Data Fig. 10f,g). We therefore focused on this line and further optimized the protocols to improve transformation efficiency. We performed heat-shock (46 °C for 3 min) and cold-shock (ice bath for 1 min) treatment of freshly isolated immature embryos (around 1.5 mm in length) to promote their transformation competence. Acetosyringone and vitamin C were added to N6 infection and co-cultivation media to enhance *Agrobacterium* infection efficiency. To promote the production of type-II callus, 2,4-dichlorophenoxyacetic acid, picloram and silver nitrate were added to Murashige and Skoog (MS) selection medium. We used the antibiotics ticarcillin sodium/clavulanate potassium in MS selection medium to inhibit *Agrobacterium* growth and reduce callus browning. Zeatin was used in Linsmaier and Skoog (LS) regeneration medium to promote shoot regeneration. To promote root induction and growth, half-strength MS medium was used for rooting medium with indole-3-butyric acid (IBA) and 1-naphthaleneacetic acid (NAA) added. We finally achieved an average of 3.21% transformation efficiency for infected embryos (Extended Data Fig. 10o). Following an established method, the CRISPR–Cas9 cassette targeting *lac1* was directly transformed into HI3. The HI3 plants carrying the CRISPR–Cas9 cassette targeting *lac1* were crossed with different maize inbred lines to generate gene-edited haploids in these inbred line backgrounds. The gene-edited haploids were then doubled using the mitotic inhibitor colchicine. Primer sequences used in constructing transgenic vectors are listed in Supplementary Table 4 and 5.

Yeast one-hybrid assays

Yeast one-hybrid assays were performed as previously described[45]. In brief, the full-length coding sequence of *RAVL1* was amplified and cloned into the pB42AD vector (Clontech), generating the AD–RAVL1 plasmid. The plasmid for AD fusion was co-transformed with the *LacZ* reporter vector (*pLacZi2μ*) driven by the *lac1* and *D11* promoter into the yeast strain EGY48. These transformants were cultured at 30 °C for 12–24 h on proper dropout plates containing X-gal (5-bromo-4-chloro-3-indolyl-β-D-galactopyranoside). Yeast transformation was performed following the Yeast Protocols Handbook (Clontech). The sequences of primers used in yeast one-hybrid are listed in Supplementary Table 5.

Recombinant protein expression and purification

To generate His-tagged RAVL1 protein, the full-length coding sequence of *RAVL1* was amplified and cloned into the pET-32a vector (Novagen) at the EcoR1 and Xho1 restriction sites. To generate His–phyA1-C protein, the C-terminal corresponding coding sequences were amplified and cloned into the PET28a vector (Novagen). To generate the constructs expressing GST–phyA1, GST–phyA1–N, GST–phyA2 and GST–phyA2–N, the corresponding coding sequences were amplified and cloned into the pGEX-4T-1 vector (Amersham Biosciences). All constructs were transformed into the *Escherichia coli* Rosetta cells (DE3). Expression of the His–RAVL1 fusion protein was induced by adding 0.8 mM isopropyl-β-D-thiogalactoside (IPTG) and cells were incubated at 16 °C for more than 12 h with shaking. Fusion proteins of His–phyA1–C, GST–phyA1, GST–phyA1–N, GST–phyA2 and GST–phyA2–N were induced by adding 0.8 mM IPTG and incubated at 37 °C for 4 h with shaking. The fusion proteins were purified using IDA-Nickel beads (BeaverBeads, 70501-5) and Glutathione Sepharose beads (BeaverBeads, 70601-5) according to the manufacturer's instructions. The sequences of primers used in protein expression are listed in Supplementary Table 5.

Electrophoretic mobility shift assays

The promoter probes were amplified using primers labelled with biotin at the 5′ end (Supplementary Table 6). EMSAs were performed using a Light Shift Chemiluminescent EMSA Kit (Thermo Fisher Scientific, No. 20148) according to the manufacturer's instructions with minor modifications. In brief, 40 ng of purified fusion protein (His–RAVL1) was incubated with 4 ng or 6 ng of biotin-labelled or unlabelled probes in 20 μl of binding reaction mixture containing 1× binding buffer, 2.5% (v/v) glycerol, 5 mM $MgCl_2$, 0.05% (w/v) NP-40 and 50 ng ml^{-1} Poly(dI-dC) for 20 min at room temperature. The binding reactions were then stopped by adding 5× native sample loading buffer, separated on 6% native polyacrylamide, membranes (Millipore) and photographed by Qinxiang Chemiluminescent Imaging System (ChemiScope6000).

Split firefly luciferase complementation assay

The split firefly luciferase complementation imaging assays (LCI) were performed in *N. benthamiana* leaves as previously described[46]. In brief, the full-length coding sequences of *GUS*, *phyA* and *phyB* without respective stop codons were cloned into *p35S:nLUC*, forming the GUS-nLUC, phyA-nLUC and phyB-nLUC constructs, respectively. The full-length coding sequences of GUS and RAVL1 were cloned into *p35S:cLUC*, forming the GUS-cLUC and RAVL1-cLUC construct, respectively. The constructs were co-infiltrated into *N. benthamiana* leaves. After infiltration, plants were cultured for 48 h under a 16:8 h light–dark cycle. A Chemiluminescent Imaging System (Tanon-5200) was used to capture the chemiluminescence signals. The primers used in LCI are listed in Supplementary Table 5.

In vitro pull-down assay

For in vitro binding, both the purified recombinant bait proteins (His–RAVL1 and His) and prey proteins (GST–phyA1, GST–phyA2, GST–phyA1–N and GST–phyA2–N) were added into 1 ml binding buffer (1× PBS, 0.1% v/v Nonidet P-40, 2 mM dithiothreitol, 1× EDTA-free complete protease inhibitor Cocktail (Roche)) and then incubated at 4 °C for 2 h. IDA-Nickel beads (BeaverBeads, 70501-5) were then added and the mixture was incubated for 1 h at 4 °C. After washing 5 or 6 times with binding buffer, the pull-down proteins were eluted by 2× SDS loading buffer at 100 °C for 10 min. The interaction signal was detected by immunoblotting with His antibody (YEASEN, 1:6,000 dilution) and GST antibody (ABclonal, 1:6,000 dilution).

Co-immunoprecipitation assay

Co-immunoprecipitation assays were performed as previously described[47]. In brief, the full-length coding sequences of *RAVL1*, *phyA1* and *phyA2* without stop codons were amplified from the inbred line B73 and recombined into pSuper:1300-MYC/GFP using the Sal1 and Spe1 restriction sites, generating pSuper:RAVL1-MYC, pSuper:phyA1-GFP and phyA2-GFP fusion plasmids. These fusion plasmids were transformed into *A. tumefaciens* strain GV3101 containing P19 and co-infiltrated into tobacco leaves. The empty vector pSuper:1300-GFP was used as a negative control. After culturing for two days at 25 °C, total proteins from tobacco leaves were extracted using protein extraction buffer (50 mM Tris-HCl pH 7.5, 150 mM NaCl, 10 mM $MgCl_2$, 1 mM EDTA, 0.1% v/v NP-40, 1 mM PMSF, 50 μM MG132, and 1× EDTA-free complete protease inhibitor cocktail (Roche)). The extracted proteins were equally divided into two parts. One part was exposed to 5 min of far-red light alone, and the other part was exposed to 5 min of far-red light immediately followed by 5 min of red light. The proteins were then incubated with GFP agarose beads (Alpalife) for 2.5 h at 4 °C in darkness. Beads were then gently washed 3 or 4 times with washing buffer (50 mM Tris-HCl pH 7.5, 150 mM NaCl, 10 mM $MgCl_2$ and 1 mM EDTA), and the immunoprecipitated proteins were detected with anti-MYC (MBL, 1:6,000 dilution) and anti-GFP (TransGen, 1:6,000 dilution).

Generation of anti-RAVL1 and anti-phyA and immunoblotting

The antibody against RAVL1 was generated in rabbit using a synthetic specific peptide with the sequence FIDWKRRADSRDPHR (corresponding to residues 192–206 of RAVL1) as the antigen, according to the standard protocol of Shanghai Youke Biotechnology. The antibody against phyA was generated in rabbit using His–phyA1-C protein as antigens, according to the standard protocol of Beijing Protein Innovation. To examine how RAVL1 and phyA are regulated by shade, both

long-term and short-term shade treatments were performed for the seedlings of wild-type and *phyA*-knockout lines. For long-term shade treatment, the *phyA*-knockout lines and the wide type were planted in white light (low-red:far-red = 9, photosynthetic photon flux density (PPFD) = 70 μmol m^{-2} s^{-1}) or simulated shade (low-red:far-red = 0.2, PPFD = 27 μmol m^{-2} s^{-1}) for 2 weeks. For short-term shade treatment, the *phyA*-knockout lines and the wild type were first planted under 16:8 h light–dark cycle at 25 °C for 14 days. Half of the plants were then transferred to white light and the other half were transferred to simulated shade conditions (low-red:far-red = 0.2). Leaf samples were collected at Zeitgeber times 0, 1, 2, 4, 6 and 12. Total proteins of all samples were extracted with protein extraction buffer (12.5 mM sodium borate buffer, 1% w/v SDS, 2% v/v β-mercaptoethanol, 1 mM PMSF, 20 μM MG132, 1 × EDTA-free complete protease inhibitor cocktail (Roche)). The proteins were detected with RAVL1 antibody at a dilution of 1:1,500 at room temperature for 3 h, and detected with phyA antibody at a dilution of 1:1,000 at 37 °C for 3 h. Immunoblot results were quantified using ImageJ (1.54d).

Cell-free protein degradation assay

Cell-free protein degradation assays were performed as previously described[48,49]. In brief, His-tagged RAVL1 protein was purified from *E. coli*. Total proteins were extracted in the dark from the leaves of 14-day-old maize seedlings (grown under white light and shade, respectively) with degradation buffer (50 mM Tris-HCl pH 8.0; 10 mM EDTA pH 8.0; 1 mM $MgCl_2$; 0.5 M sucrose and 2 mM DTT). Equal amounts of total proteins from wild-type (white), wild-type (shade) and *phyA*-KO1 plants were incubated with His-tagged RAVL1 protein at 25 °C for 12 min and 24 min, with or without the proteasome inhibitor MG132 (final concentration 50 μM). The reactions were stopped by adding 5× SDS sample loading buffer and boiled for 10 min. RAVL1 protein was detected by immunoblotting with the His antibody (YEASEN, 1:6,000 dilution).

Transient expression assays

For the dual-luciferase transient-expression assays, a 2.66-kb *lac1* promoter segment and a 2.88-kb *D11* promoter segment were separately amplified from the inbred line B73 and recombined into pGreenII 0800-LUC vectors at Kpn1 and PstI sites, forming the $lac1_{pro}$:*LUC* and $D11_{pro}$:*LUC* fusion plasmids, respectively. The plasmids were transformed separately into *A. tumefaciens* strain GV3101 containing the helper plasmid pSoup-P19. The full-length coding sequences of *RAVL1*, *phyA1* and *phyA2* were amplified and recombined into pGreenII 62-SK vector at EcoR1 and Xho1 sites, driven by the 35S promoter, to generate RAVL1, phyA1 and phyA2 effectors. The dual-luciferase transient-expression assays in maize protoplasts were carried out as previously described[10,48,49]. In brief, the RAVL1 effector was co-transformed with $lac1_{pro}$:*LUC* or $D11_{pro}$:*LUC* reporters into protoplasts isolated from the leaves of 2-week-old etiolated seedling of the inbred line B73. The empty vector pGreenII 62-SK was used as a control. The dual-luciferase transient-expression assays in tobacco leaves were performed as previously described[48]. *A. tumefaciens* strain GV3101 containing $Super_{pro}$:RAVL1–MYC, $Super_{pro}$:phyA1–GFP, $Super_{pro}$:phyA2–GFP fusion plasmids and the $lac1_{pro}$:*LUC* or $D11_{pro}$:*LUC* plasmids were infiltrated into fully expanded tobacco leaves. The infiltrated plants were grown at 25 °C under 16:8 h light–dark cycles for 48 h. The empty vectors pSuper:1300-MYC and pSuper:1300-GFP were used as negative controls. Total proteins were extracted from the samples. Luciferase signals were detected using dual-luciferase assay reagents (Promega) following the manufacturer's instructions. The sequences of primers used in the transient expression assay are listed in Supplementary Table 5.

Chromatin immunoprecipitation assays

ChIP assays were conducted following a previously reported protocol[50] with minor modifications. In brief, the $Super_{pro}$:RAVL1–MYC fusion plasmids were transformed into maize protoplasts, which were isolated from the leaves of two-week-old etiolated seedling of inbred line B73. The empty vector pSuper:1300-MYC was used as a negative control. The protoplasts were cross-linked using 1% v/v formaldehyde, and chromatin was extracted from the cross-linked samples and fragmented using an ultrasonicator (SCIENTZ-IID). DNA fragments associated with RAVL1–MYC protein were incubated with MYC agarose beads (Alpalife). ChIP–qPCR was performed to detect the immunoprecipitated chromatin using specific primers (Supplementary Table 4). The following formula[51] was used to calculate the percentage of immunoprecipitated fragment (IP%): IP% = 2 (−ΔCt (normalized ChIP)), in which ΔCt = (Ct (ChIP) − (Ct (Input) − $\log_2$(input dilution factor))) and input dilution factor = (fraction of the input chromatin saved)$^{-1}$.

Field trials under different planting densities

Field trials were carried out as previously described[10] and were conducted in Tieling (41.5° N, 123.2° E), Sanya (18.2° N, 109.1° E) and Beijing (Shangzhuang and Tongzhou, 39.9° N, 116.4° E), China from 2020 to 2023. The planting time of the field trials in Tieling and Beijing was early May, and the planting time of the field trials in Sanya was the middle of November. A split-plot design with three replicates was used in all field trials (see Supplementary Fig. 1 for an example). Plant densities were randomized in the main plots and genotypes were subplots. Each subplot contained five rows. Each row was 5 m long and the row spacing was 50 cm. Routine field management was applied in fertilization, irrigation and weeding in each field trial. At maturity, all ears from the middle three rows in each subplot were harvested and phenotyped. The data were analysed using PROC MIXED with Fisher's least significant difference test in SAS (v.9.2; SAS Institute).

Measurement of photosynthetic parameters

PAR was measured using a LI-1500 Light Sensor Logger (LI-COR Biosciences) one week after pollination. The fraction of penetrated PAR is calculated as the ratio between the transmitted PAR measured at different vertical-canopy layers and the PAR values measured above the canopy[52]. PAR was measured at two vertical-canopy layers, including the layer at the ear leaf and the layer at 10 cm above the soil surface. The gas-exchange measurement was performed as described previously[53] using a LI-COR 6400XT instrument (LI-COR Biosciences). The net photosynthesis of ear leaves under different planting densities was measured, in which the PPFD was set to 1,200 μmol m^{-2} s^{-1}, the flow was set 500 ml s^{-1}, the leaf temperature was set 25 °C, and the concentration of CO_2 in the atmosphere (about 400 ppm) was used. To record the light-response curve of photosynthesis, a series of PPFD was set from 0 to 2,000 μmol m^{-2} s^{-1}, the flow was set 500 ml s^{-1}, the leaf temperature was set 25 °C, and the atmospheric CO_2 concentration was used. The light-response curves were fitted using the rectangular hyperbola model as previously described[53,54]. For the CO_2-response curve of photosynthesis, the PPFD was set 1,200 μmol m^{-2} s^{-1}, a series of CO_2 concentration was set from 400 to 0 ppm and then increased from 200 to 1,000 ppm, the flow was set 500 ml s^{-1} and the leaf temperature was set 25 °C. CO_2-response curves were fitted using the rectangular hyperbola model as previously described[55].

Quantification of brassinosteroids

The mutant *lac1* and the wild-type W22 were grown in field. The ligular regions of *lac1* and wild type were sampled at V5, V9 and V13 stages. The collected samples were immediately frozen in liquid nitrogen, then ground and quickly weighed. The weighed samples were extracted with acetonitrile, dehydrated with anhydrous NaCl and $MgSO_4$ and cleaned up using liquid–liquid extraction. The endogenous brassinosteroid contents were determined by Wuhan Greensword Creation Technology Company (http://wwwgreenswordcreation.com) using HPLC–MS/MS as described previously[56].

Haploid-induction editing

A set of 43 diverse maize inbred lines were used to perform haploid-induction editing, including 23 public academic lines, eight parents of hybrids widely planted in China, and 12 breeding lines provided by Hainan Aoyu Biotechnology (Supplementary Table 2). The haploid inducer HI3 contains four widely used colour markers for haploid identification, including a purple scutellum in the embryo, a purple aleurone layer in the endosperm, purple roots and purple leaf sheaths[30]. The pollen from *lac1*-edited HI3 plants were collected to pollinate the 43 inbred lines. From the resulting F_1 seeds, seeds with a colourless scutellum and a pigmented aleurone were haploids; otherwise, they were deemed diploids. The putative haploids (D_0 seeds) were germinated on paper towels until their coleoptiles were about 2-cm long. Coleoptile tips were cut off and immersed in colchicine (0.06% colchicine + 2% DMSO) to promote chromosomal doubling. Subsequently, D_0 seedlings were washed and planted in trays in the greenhouse for recovery. When D_0 seedlings grew to the V2 stage, they were transplanted to field, during which seedlings with purple roots were discarded. In the field, plants with purple leaf sheaths were further removed. Around the V7 stage, leaf tips of D_0 plants were daubed with herbicide and phosphinothricin-resistant (*Cas9*-positive) plants were removed from the field (Supplementary Fig. 2a). The remaining D_0 plants were then sampled and genotyped with *Cas9* transgene-specific primers (Supplementary Fig. 2b). A total of 1,175 D_0 plants for 43 inbred lines were obtained. Leaf DNA isolated from the D_0 plants from the same inbred were pooled together and sequenced to check whether they contain the inducer allele *matl* (Supplementary Fig. 2c), a 4-bp insertion in *MATL/NLD/ZmPLA1*[31–33]. The 1,175 D_0 plants were finally sequenced to identify potential edits in *lac1* (Supplementary Fig. 3). D_0 plants carrying homozygous *lac1* mutations were self-pollinated to get D_1 seeds for subsequent field phenotyping.

Reporting summary

Further information on research design is available in the Nature Portfolio Reporting Summary linked to this article.

Data availability

All data are available within this Article and its Supplementary Information. Microsoft Excel 2016, R software (v.4.3.2) and SAS (v.9.2) were used for statistical analyses (two-tailed Student's *t*-test, correlation analysis, one-way and two-way ANOVA, and mixed linear model analysis). Uncropped gel images are provided in Supplementary Figs. 6–8. Source data are provided with this paper.

40. Schmittgen, T. D. & Livak, K. J. Analyzing real-time PCR data by the comparative C_T method. *Nat. Protoc.* **3**, 1101–1108 (2008).
41. Yang, Q. et al. CACTA-like transposable element in *ZmCCT* attenuated photoperiod sensitivity and accelerated the postdomestication spread of maize. *Proc. Natl Acad. Sci. USA* **110**, 16969–16974 (2013).
42. Raji, J. A., Frame, B., Little, D., Santoso, T. J. & Wang, K. in *Maize: Methods and Protocols* (ed. Lagrimini L. M.) 15–40 (Springer, 2018).
43. Ishida, Y., Hiei, Y. & Komari, T. *Agrobacterium*-mediated transformation of maize. *Nat. Protoc.* **2**, 1614–1621 (2007).
44. Frame, B. R. et al. Improved *Agrobacterium*-mediated transformation of three maize inbred lines using MS salts. *Plant Cell Rep.* **25**, 1024–1034 (2006).
45. Lin, R. C. et al. Transposase-derived transcription factors regulate light signaling in *Arabidopsis*. *Science* **318**, 1302–1305 (2007).
46. Chen, H. M. et al. Firefly luciferase complementation imaging assay for protein–protein interactions in plants. *Plant Physiol.* **146**, 368–376 (2008).
47. Yan, Y. et al. MYB30 is a key negative regulator of *Arabidopsis* photomorphogenic development that promotes PIF4 and PIF5 protein accumulation in the light. *Plant Cell* **32**, 2196–2215 (2020).
48. Li, Z. Y. et al. The transcription factor *bZIP68* negatively regulates cold tolerance in maize. *Plant Cell* **34**, 2833–2851 (2022).
49. Peng, J. et al. COP1 positively regulates ABA signaling during *Arabidopsis* seedling growth in darkness by mediating ABA-induced ABI5 accumulation. *Plant Cell* **34**, 2286–2308 (2022).
50. Kaufmann, K. et al. Chromatin immunoprecipitation (ChIP) of plant transcription factors followed by sequencing (ChIP-SEQ) or hybridization to whole genome arrays (ChIP-CHIP). *Nat. Protoc.* **5**, 457–472 (2010).
51. Haring, M. et al. Chromatin immunoprecipitation: optimization, quantitative analysis and data normalization. *Plant Methods* **3**, 16 (2007).
52. Du, X. B., Wang, Z., Lei, W. X. & Kong, L. C. Increased planting density combined with reduced nitrogen rate to achieve high yield in maize. *Sci. Rep.* **11**, 12 (2021).
53. Wei, S. B. et al. A transcriptional regulator that boosts grain yields and shortens the growth duration of rice. *Science* **377**, 386–396 (2022).
54. Ye, Z. P. A new model for relationship between irradiance and the rate of photosynthesis in *Oryza sativa*. *Photosynthetica* **45**, 637–640 (2007).
55. Baly, E. C. C. The kinetics of photosynthesis. *Proc. R. Soc. B* **117**, 218–239 (1935).
56. Ding, J., Mao, L. J., Wang, S. T., Yuan, B. F. & Feng, Y. Q. Determination of endogenous brassinosteroids in plant tissues using solid-phase extraction with double layered cartridge followed by high-performance liquid chromatography-tandem mass spectrometry. *Phytochem. Anal.* **24**, 386–394 (2013).

Acknowledgements This research was supported by the National Natural Science Foundation of China (32025027, 32330077, 91935305 and 32225006), the National Key Research and Development Program of China (2022YFD1201503), Hainan Yazhou Bay Seed Laboratory (B21HJ0111), Pinduoduo-China Agricultural University Research Fund (PC2023A01003), Sanya Yazhouwan Science and Technology City Administration (SYND-2022-26), the Chinese Universities Scientific Fund (2020TC149 and 2022TC138) and China National Postdoctoral Program for Innovative Talents (BX20200373).

Author contributions J.T., C.W. and F.C. contributed equally to this work. C.W., J.T. and F.T. designed the research. J.T., C.W. and F.C. performed most of the experiments and analysed the data. J.T., C.W., F.C., W.Q., H.Y., S.Z., J.X., X.D., Y.Z. and L.W. collected phenotypic data. J.L., Y.C. and H.L. helped with experiments on phyA function. J.Z. and M.Z. contributed to the maize transgenic experiments. H.Z. and D.D. performed the genetic transformation of haploid inducers. S.C. helped with experiments on haploid induction. Q.C. helped with statistical analysis. X.W.D. provided helpful advice on manuscript preparation. J.T., C.W., J.L. and F.T. wrote and edited the manuscript. All authors read and approved the final manuscript.

Competing interests A patent on the use of *lac1* has been filed in China by F.T., C.W. and J.T. (202311558593.9). A patent on the haploid-inducer genetic transformation and haploid-induction editing has been filed in China by F.T., D.D., C.W., H.Z. and S.C. (202311568051.X). D.D. and H.Z. are employees of Hainan Aoyu Biotechnology, which develops maize lines for commercial use. The other authors declare no competing interests.

Additional information

Supplementary information The online version contains supplementary material available at https://doi.org/10.1038/s41586-024-07669-6.

Correspondence and requests for materials should be addressed to Jigang Li or Feng Tian.

Peer review information *Nature* thanks James Holland and the other, anonymous, reviewer(s) for their contribution to the peer review of this work.

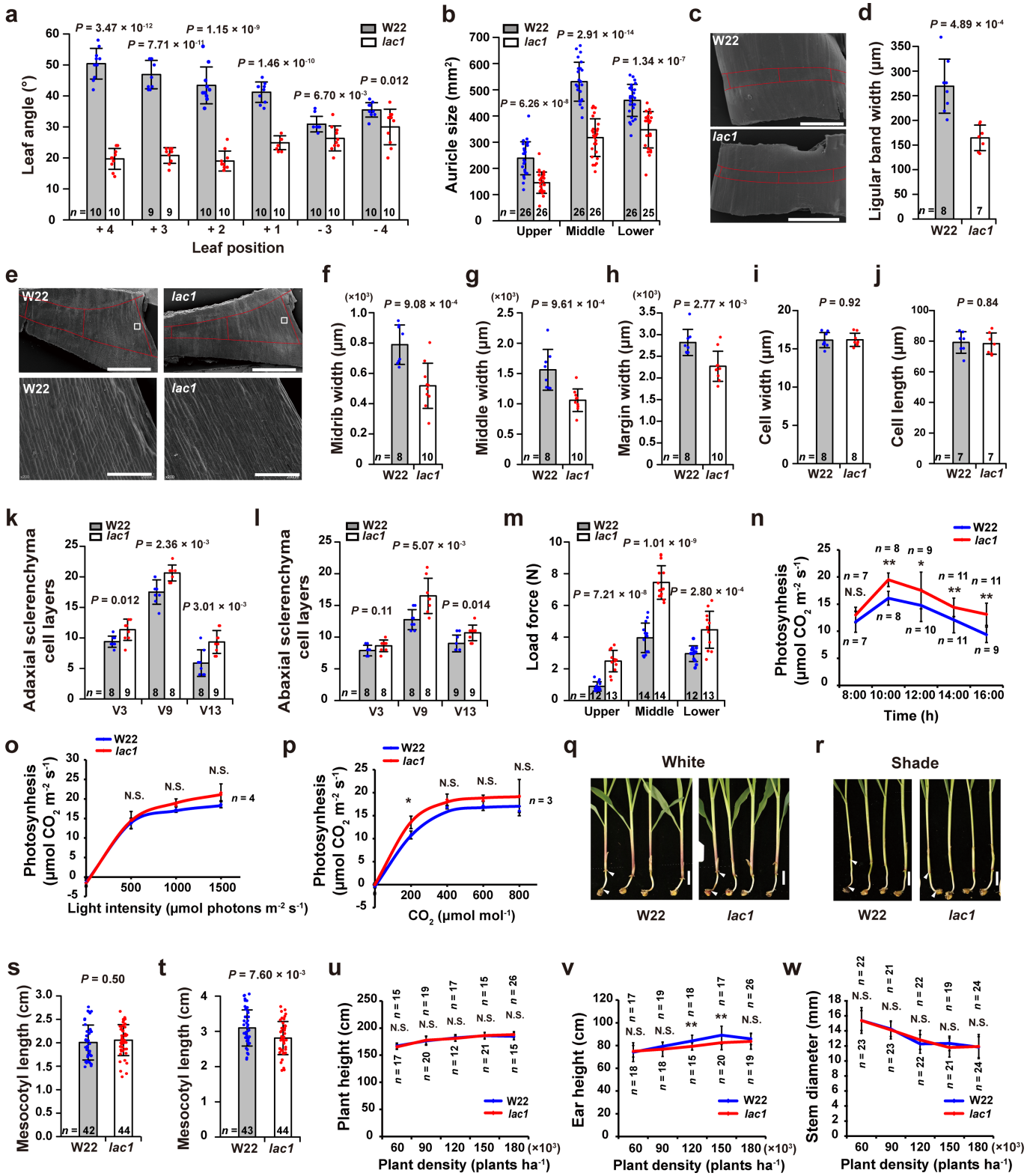

Extended Data Fig. 1 | See next page for caption.

Extended Data Fig. 1 | Phenotypic characterization of *lac1*. **a**, Comparison of leaf angles throughout the entire canopy leaves between *lac1* and wild-type W22 under the planting density of 90,000 plants per hectare. The positive and negative numbers indicate the leaves above and below the primary ear, respectively. **b**, Comparison of auricle area in upper, middle and lower leaves between *lac1* and W22. **c**, Scanning electron microscopy analysis of the ligular regions of *lac1* and W22. Scale bar = 1 mm. **d**, Comparison of the ligular band width between *lac1* and W22. **e**, Scanning electron microscopy analysis of the mature ligular regions of *lac1* and W22. Scale bars = 2 mm (top) and 200 μm (bottom). **f**-**h**, Comparison of the width of the midrib (**f**), the middle region (**g**) and the margin (**h**) of auricles between *lac1* and W22. **i**,**j**, Comparison of the cell length (**i**) and width (**j**) of auricles. **k**,**l**, Comparison of the number of the adaxial (**k**) and abaxial (**l**) sclerenchyma cell layers in the ligular regions between *lac1* and W22 sampled at V3, V9 and V13 stages. **m**, Comparison of the mechanical strength of the midrib of upper, middle and lower leaves between *lac1* and W22. **n**–**p**, The ear leaves of *lac1* plants displayed improved diurnal changes (**n**), light-response curves (**o**) and CO_2-response curves (**p**) of net photosynthesis under the density of 120,000 plants per hectare one week after pollination. **q**,**r**, Comparison of the mesocotyl length of seedlings of *lac1* and the wild type (W22) grown in white light and simulated shade (R:FR = 0.2) conditions. Scale bar = 2 cm. **s**, *lac1* and W22 seedlings have similar mesocotyl lengths in white light. **t**, The mesocotyl length of *lac1* is shorter than W22 in simulated shade. **u**–**w**, Comparison of plant height (**u**), ear height (**v**) and stem diameter (**w**) between *lac1* and W22 under different planting densities. Data are mean ± s.d. (*n* represents numbers of biologically independent samples). A two-tailed Student's *t*-test was used to determine *P* values (see Source Data). In **n**-**p**, **u**-**w**, *, $P < 0.05$. **, $P < 0.01$. N.S., non-significant.

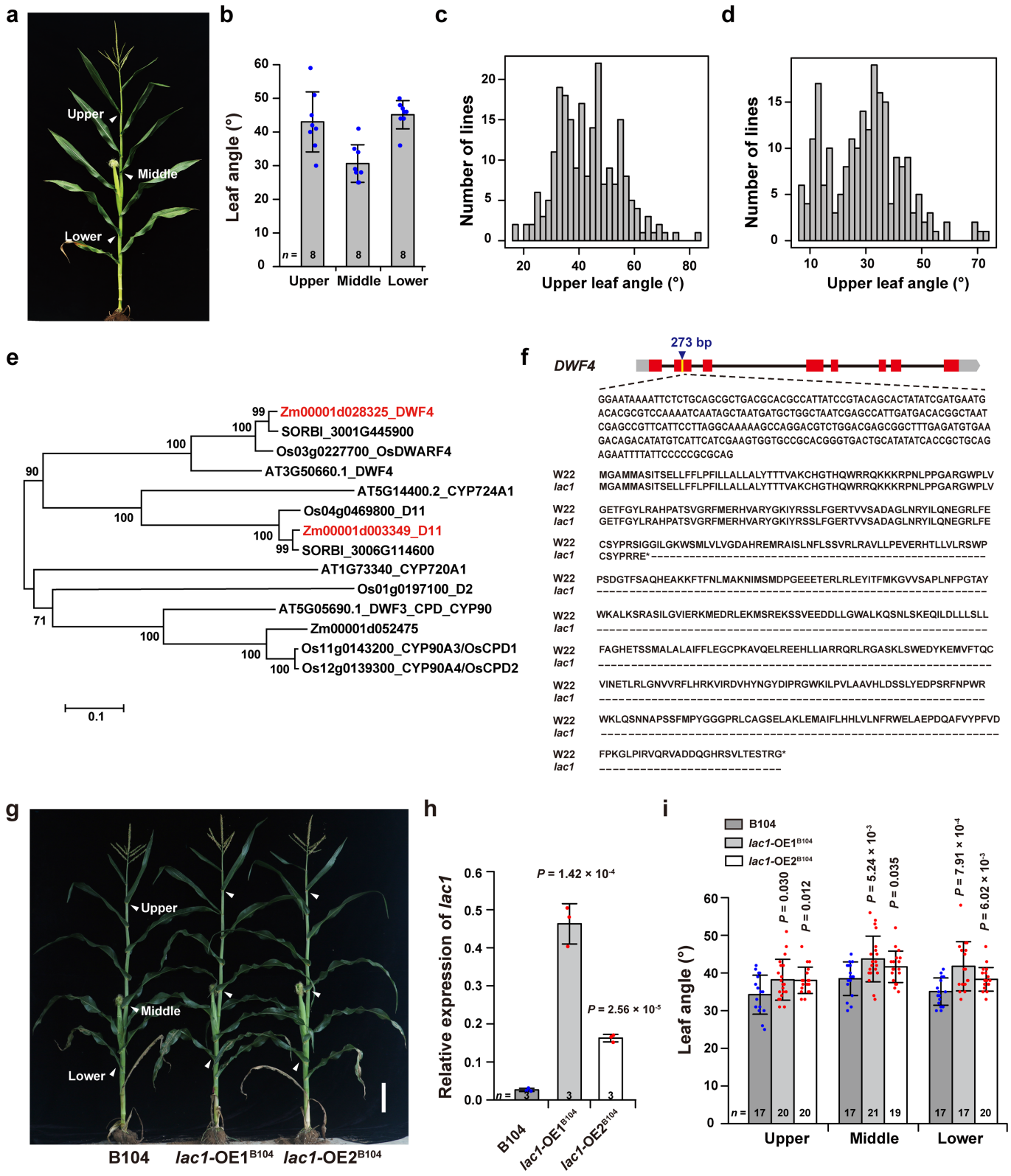

Extended Data Fig. 2 | See next page for caption.

Extended Data Fig. 2 | Map-based cloning and functional validation of *lac1*. **a**, Plant phenotypes of the inbred line Mo17. The white arrows indicate the lower, middle, and upper leaves from which leaf angle was scored. **b**, The upper, middle and lower leaf angles of the inbred line Mo17. **c**, Distribution of upper leaf angle in the F_2 populations derived from the cross of W22 × Mo17. Data are mean ± s.d. (*n* represents numbers of biologically independent samples). **d**, Distribution of upper leaf angle in the F_2 populations derived from the cross of *lac1* × Mo17. **e**, *lac1* is a homolog of *DWF4* in rice, sorghum and Arabidopsis. The phylogenetic tree was constructed by the neighbor-joining method using MEGA (version 6.0). Branch significance was tested by bootstrapping (1,000 replicates). **f**, The *lac1* mutant contains a 273-bp insertion in the second exon of *DWF4* (above) and the 273-bp insertion in *lac1* causes a truncated DWF4 protein (below). **g**, Plant phenotypes of *lac1* overexpression lines (*lac1*-OE1^{LH244} and *lac1*-OE2^{LH244}) and their wild type (B104). The white arrows indicate the lower, middle, and upper leaves from which leaf angle was scored. Scale bar = 23 cm. **h**, Expression levels of *lac1* in wild-type and *lac1* overexpression lines. The developing leaves at V2 stage were sampled for expression analysis. Data are mean ± s.d. (*n* represents numbers of biologically independent replicates). **i**, Comparison of the upper, middle and lower leaf angles between *lac1* overexpression lines (*lac1*-OE1^{LH244} and *lac1*-OE2^{LH244}) and wild-type B104 under the planting density of 82,500 plants per hectare. Data are mean ± s.d. (*n* represents numbers of biologically independent samples). In **h**,**i**, a two-tailed Student's *t*-test was used to determine *P* values (see Source Data).

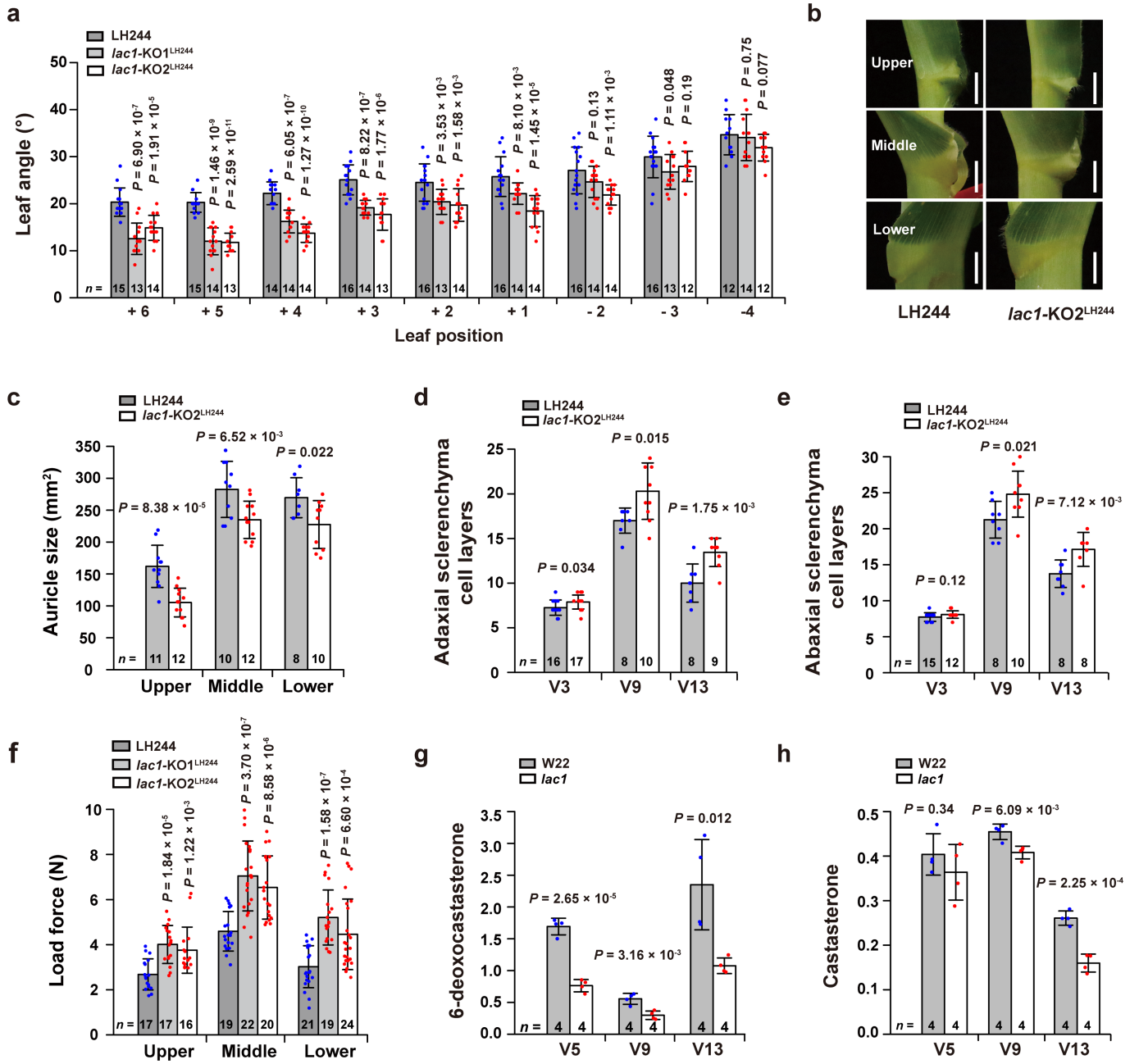

Extended Data Fig. 3 | Phenotypic characterization of *lac1* knockout lines. **a**, Comparison of leaf angles throughout the entire canopy leaves between *lac1* knockout lines (*lac1*-KO1^{LH244} and *lac1*-KO2^{LH244}) and the wild type (LH244) under the planting density of 82,500 plants per hectare. The positive and negative numbers indicate the leaves above and below the primary ear, respectively. **b**, The mature ligular regions of *lac1*-KO2^{LH244} and LH244 in upper, middle and lower leaves. Scale bars = 2 cm. **c**, Comparison of auricle area in upper, middle and lower leaves between *lac1*-KO2^{LH244} and wild-type LH244. **d**,**e**, Comparison of the number of the adaxial (**d**) and abaxial (**e**) sclerenchyma cell layers in the ligular region between *lac1*-KO2^{LH244} and LH244 sampled at V3, V9 and V13 stages. **f**, Comparison of the mechanical strength of the midrib of the upper, middle and lower leaves between *lac1* knockout lines (*lac1*-KO1^{LH244} and *lac1*-KO2^{LH244}) and LH244. **g**,**h** Comparison of the 6-deoxocastasterone (**g**) and castasterone (**h**) content in the ligular region between *lac1* and the wild type measured at V5, V9 and V13 stages. Data are mean ± s.d. (*n* represents numbers of biologically independent samples). In **a**,**c**–**h**, a two-tailed Student's *t*-test was used to determine *P* values (see Source Data).

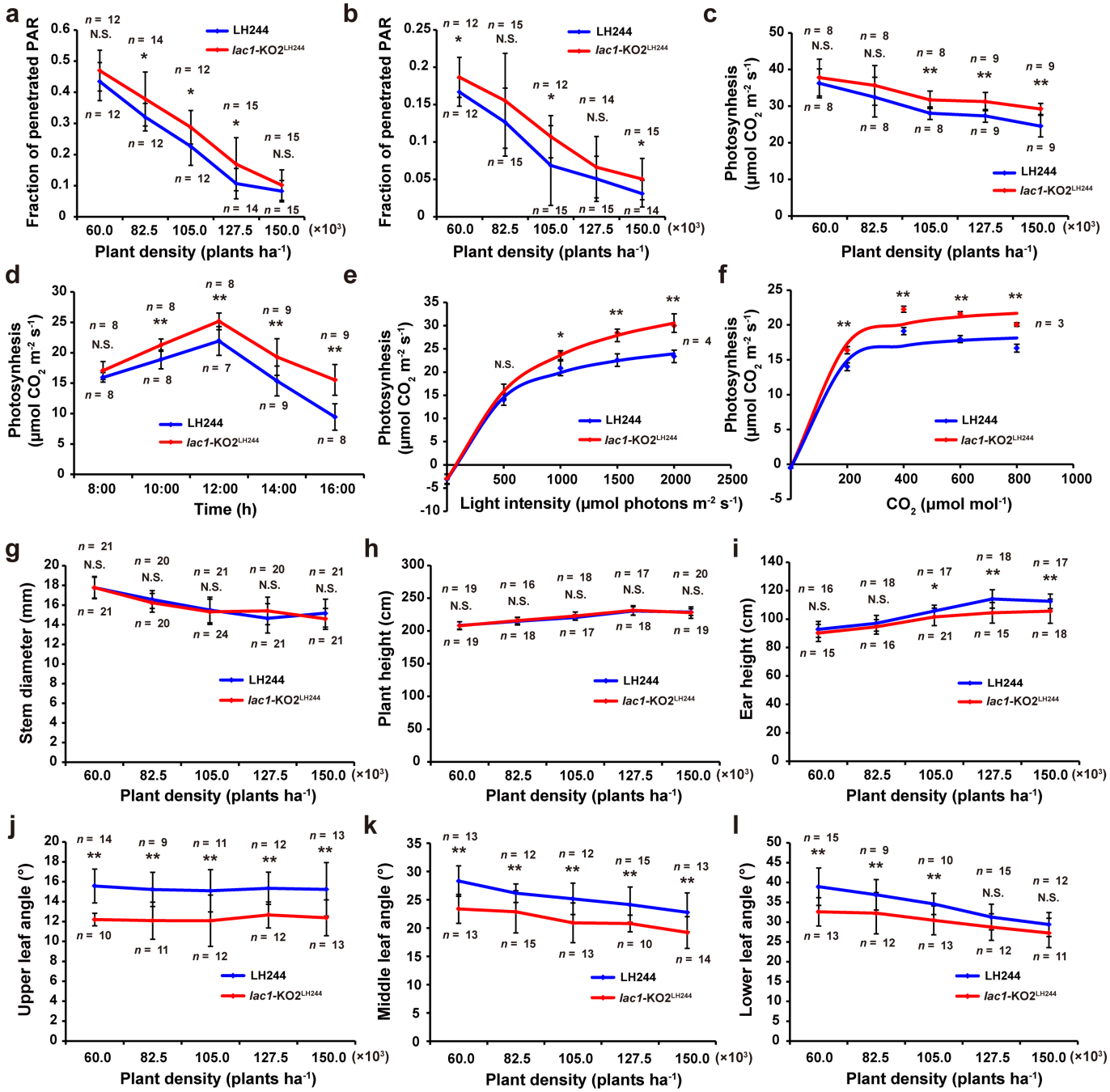

Extended Data Fig. 4 | The *lac1* knockout lines have improved photosynthetic capacity and weakened shade-avoidance responses. a,**b**, Comparison of light penetration at the layer of the ear leaf (**a**) and the layer at 10 cm above the soil surface (**b**) between *lac1*-KO2^{LH244} and the wild type (LH244) under different planting densities one week after pollination. PAR, photosynthetically active radiation. The fraction of penetrated PAR is calculated as the ratio of PAR measured at different canopy layers to PAR measured above the canopy. **c**, Comparison of net photosynthesis of the ear leaves between *lac1*-KO2^{LH244} and wild-type LH244 under different planting densities at one week after pollination. **d**–**f**, The ear leaves of *lac1*-KO2^{LH244} plants show improved diurnal changes (**d**), light-response curves (**e**) and CO_2-response curves (**f**) of net photosynthesis under the density of 105,000 plants per hectare one week after pollination. **g**–**l**, Comparison of stem diameter (**g**), plant height (**h**), ear height (**i**), upper leaf angle (**j**), middle leaf angle (**k**) and lower leaf angle (**l**) between *lac1*-KO2^{LH244} and wild-type LH244 under different planting densities. Data are mean ± s.d. (*n* represents numbers of biologically independent samples). A two-tailed Student's *t*-test was used to determine *P* values (see Source Data). *, $P < 0.05$. **, $P < 0.01$. N.S., non-significant.

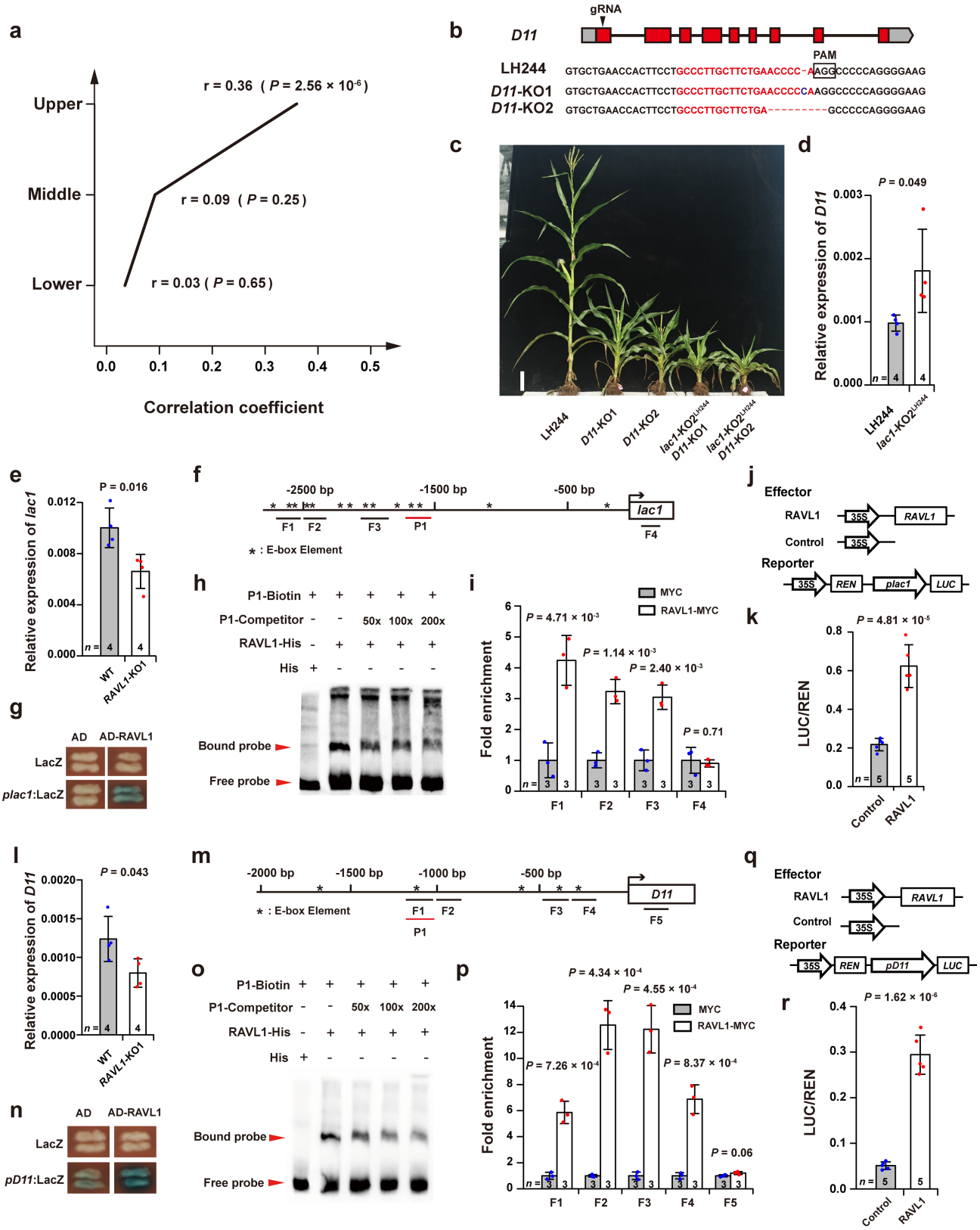

Extended Data Fig. 5 | See next page for caption.

Extended Data Fig. 5 | *lac1* and *D11* function redundantly and are directly regulated by *RAVL1*. **a**, Correlation between *lac1* expression in the ligular regions of the upper, middle and lower leaves and upper, middle and lower leaf angle in a panel of 219 maize inbred lines. Pearson's correlation coefficients and their statistical significance were determined using R. **b**, Two homozygous CRISPR–Cas9 knockout lines with a deletion or insertion in the target site of *D11*. Gene model and the wild-type sequence are shown at the top. Target site is highlighted in red, and protospacer-adjacent motif (PAM) sequence is indicated by a black rectangle. Dotted lines represent deletions. **c**, Plant phenotypes of the wild type (LH244), single mutants (*D11*-KO1 and *D11*-KO2) and double mutants (*lac1*-KO2^{LH244} *D11*-KO1 and *lac1*-KO2^{LH244} *D11*-KO2). Scale bar = 22 cm. **d**, *D11* is up-regulated in *lac1*-KO2^{LH244}. **e**,**l**, The expression of *lac1* (**e**) and *D11* (**l**) is down-regulated in *RAVL1*-KO1. **f**,**m**, Schematics of the promoters of *lac1* (**f**) and *D11* (**m**). Asterisks indicate putative E-box motifs. **g**,**n**, Yeast one-hybrid assays indicates RAVL1 can bind the promoters of *lac1* (**g**) and *D11* (**n**) in yeast. **h**,**o**, Electrophoretic-mobility shift assays (EMSA) show RAVL1 binds the putative E-box motif in the promoters of *lac1* (**h**) and *D11* (**o**). The biotin-labeled probe P1 is indicated in (**f**,**m**). Unlabeled probes were used in the competition assay. **i**,**p**, Chromatin immunoprecipitation–quantitative polymerase chain reaction (ChIP–qPCR) detected significant enrichment in the fragments containing the E-box motif in the promoters of *lac1* (**i**) and *D11* (**p**). The assayed fragments (F1–F4 in **i** and F1–F5 in **p**) are indicated in (**f**,**m**). Fold enrichment was calculated relative to input. **j**,**q**, Schematic representation of the effectors and reporter constructs used in the transient expression assays in maize protoplasts. **k**,**r**, RAVL1 activates the expression of *lac1* (**k**) and *D11* (**r**). In **d**,**e**,**l**, data are mean ± s.d. (*n* represents numbers of biologically independent replicates). In **i**,**k**,**p**,**r**, data are mean ± s.d. (*n* represents numbers of biologically independent samples). A two-tailed Student's *t*-test was used to determine *P* values (see Source Data). The experiments in **e**-**r** were repeated three times with similar results.

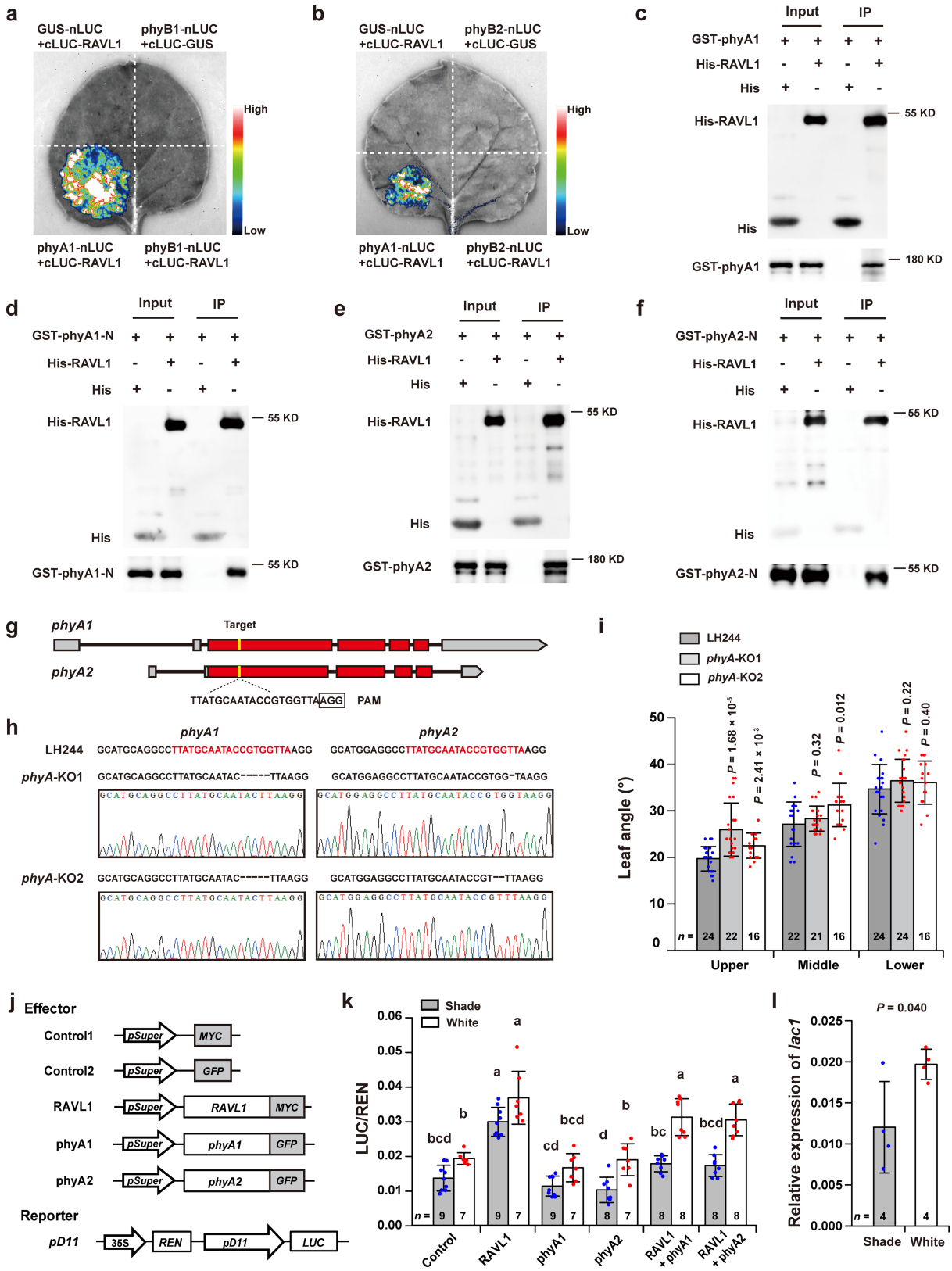

Extended Data Fig. 6 | See next page for caption.

Extended Data Fig. 6 | phyA interacts with RAVL1 and controls upper leaf angle. a,**b**, The split-firefly luciferase complementation imaging (LCI) assays in *Nicotiana benthamiana* showed that no physical interaction was detected for RAVL1 with phyB1 (**a**) and phyB2 (**b**). **c**,**d**, Pull-down assays showed that RAVL1 interacts with the full-length (**c**) and the N terminus (**d**) of phyA1 in vitro. **e**,**f**, Pull-down assays showed that RAVL1 interacts with the full-length (**e**) and the N terminus (**f**) of phyA2 in vitro. **g**, The maize genome contains two *phyA* genes (*phyA1* and *phyA2*). A conserved gRNA that edits both *phyA1* and *phyA2* was designed. The protospacer-adjacent motif (PAM) sequence is indicated by the black box. **h**, Two homozygous double mutants for *phyA1* and *phyA2* (*phyA*-KO1 and *phyA*-KO2) with deletions in the target site of *phyA1* and *phyA2*. Target site is highlighted in red. Dashed lines represent deletions. **i**, Comparison of the upper, middle and lower leaf angles between *phyA1 phyA2* double mutants and the wild type (LH244) under the planting density of 82,500 plants per hectare. **j**, Schematic representation of the effectors and reporter constructs used in the transient expression assays in tobacco leaves. **k**, phyA1 and phyA2 repress RAVL1 to activate the *D11* promoter in shade. **l**, The relative expression level of *lac1* in wild-type seedlings grown in white light and simulated shade conditions. Data are mean ± s.d. (*n* represents numbers of biologically independent replicates). In **i**,**k**, data are mean ± s.d. (*n* represents numbers of biologically independent samples). In **i**,**l**, a two-tailed Student's *t*-test was used to determine *P* values (see Source Data). In **k**, different letters indicate statistically significant differences ($P < 0.05$, two-way ANOVA with Tukey's test). All experiments were repeated three times with similar results.

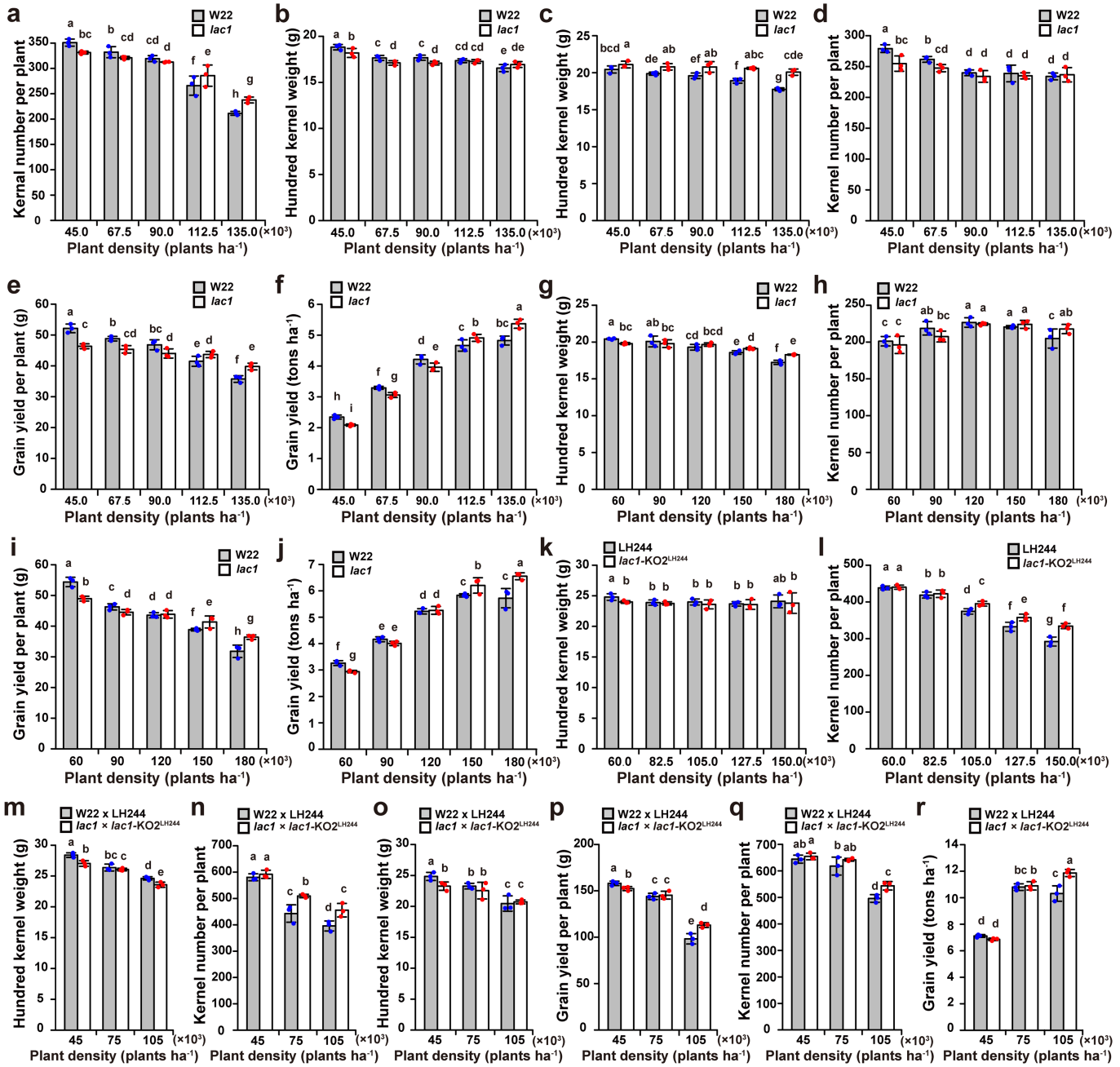

Extended Data Fig. 7 | *lac1* enhances maize yields under high-density planting. a,**b**, Comparison of kernel number per plant (**a**) and hundred kernel weight (**b**) between *lac1* and W22 under five different planting densities in Tieling in 2020. **c**-**f**, Comparison of hundred-kernel weight (**c**), kernel number per plant (**d**), grain yield per plant (**e**) and grain yield per hectare (**f**) between *lac1* and W22 under five different planting densities in Tieling in 2021. **g**-**j**, Comparison of hundred kernel weight (**g**), kernel number per plant (**h**), grain yield per plant (**i**) and grain yield per hectare (**j**) between *lac1* and W22 under five different planting densities in Sanya, China, in 2021. **k**,**l**, Comparison of hundred kernel weight (**k**) and kernel number per plant (**l**) between *lac1*-KO2^{LH244} and wild-type LH244 under five different planting densities in Tongzhou, China, in 2022. **m**,**n**, Comparison of hundred-kernel weight (**m**) and kernel number per plant (**n**) between the F_1 hybrid of *lac1* × *lac1*-KO2^{LH244} and its wild-type combination of W22 × LH244 under different planting densities in Shangzhuang, China, in 2022. **o**–**r**, Comparison of hundred kernel weight (**o**), grain yield per plant (**p**), kernel number per plant (**q**) and grain yield per hectare (**r**) between the F_1 hybrid of *lac1* × *lac1*-KO2^{LH244} and its wild-type combination of W22 × LH244 under different planting densities in Tongzhou, China, in 2022. Data are mean ± s.d. (n = 3 biological replicates in a split-plot design). Different letters indicate statistically significant differences (P < 0.05, PROC MIXED with Fisher's Least Significant Difference test in SAS).

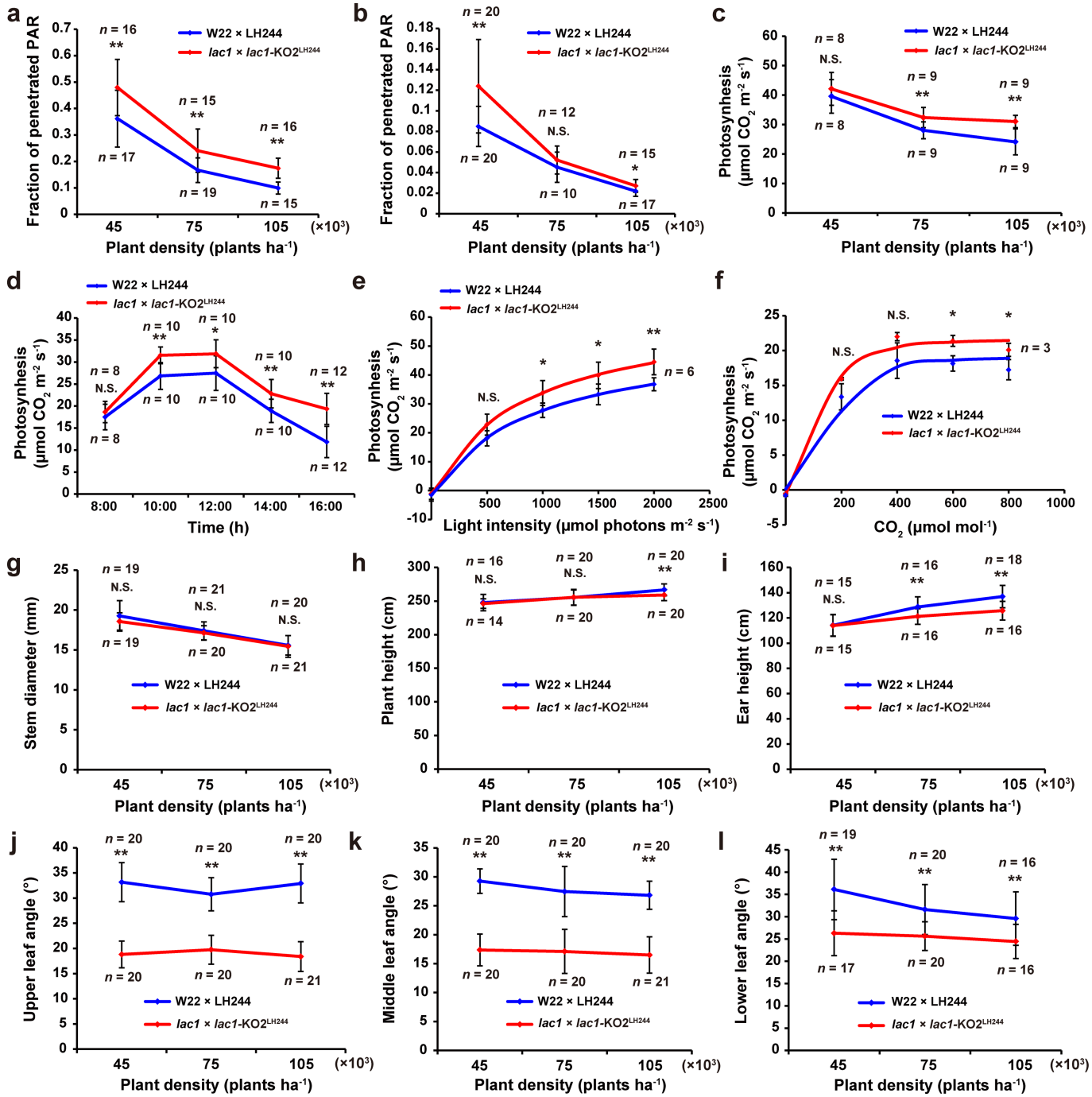

Extended Data Fig. 8 | The F_1 hybrid of *lac1* × *lac1*-KO2^{LH244} has improved photosynthetic capacity and weakened shade-avoidance responses. **a**,**b**, Comparison of light penetration at the layer of the ear leaf (**a**) and the layer at 10 cm above the soil surface (**b**) between the F_1 hybrid of *lac1* × *lac1*-KO2^{LH244} and its wild-type combination of W22 × LH244 under different planting densities one week after pollination. PAR, photosynthetically active radiation. The fraction of penetrated PAR is calculated as the ratio of the PAR measured at different canopy layers to the PAR measured above the canopy. **c**, Comparison of net photosynthesis of the ear leaves between the F_1 hybrid of *lac1* × *lac1*-KO2^{LH244} and its wild-type combination of W22 × LH244 under different planting densities one week after pollination. **d**-**f**, The ear leaves of the F_1 hybrid of *lac1* × *lac1*-KO2^{LH244} showed improved diurnal changes (**d**), light-response curves (**e**) and CO_2-response curves (**f**) of net photosynthesis under the density of 105,000 plants per hectare one week after pollination. **g**-**l**, Comparison of stem diameter (**g**), plant height (**h**), ear height (**i**), upper-leaf angle (**j**), middle leaf angle (**k**) and lower leaf angle (**l**) between the F_1 hybrid of *lac1* × *lac1*-KO2^{LH244} and its wild-type combination of W22 × LH244 under different planting densities. Data are mean ± s.d. (*n* represents numbers of biologically independent samples). A two-tailed Student's *t*-test was used to determine *P* values (see Source Data). *, $P < 0.05$. **, $P < 0.01$. N.S., non-significant.

a

The allele at *lac1* or *RAVL1*	$RAVL1^{W22}$	$RAVL1^{teosinte}$
$lac1^{W22}$	$lac1^{W22}\,RAVL1^{W22}$	$lac1^{W22}\,RAVL1^{teosinte}$
$lac1^{mutant}$	$lac1^{mutant}\,RAVL1^{W22}$	$lac1^{mutant}\,RAVL1^{teosinte}$

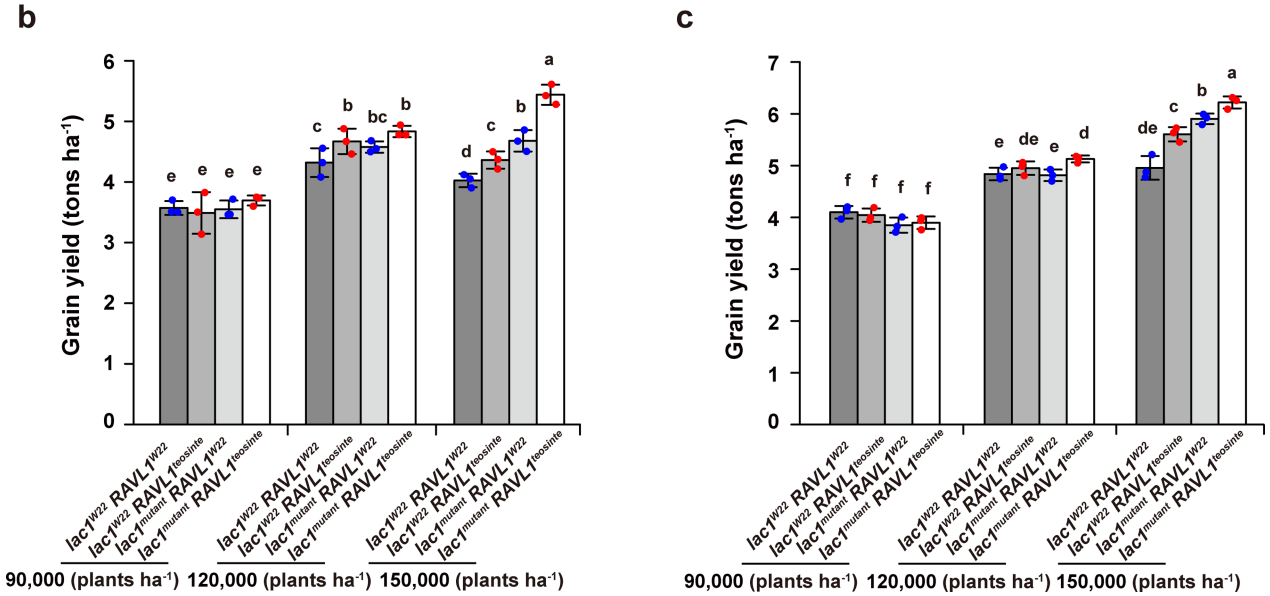

Extended Data Fig. 9 | Field trials for the four genotype combinations of *lac1* and *RAVL1*. **a**, The four genotype combinations were derived from the cross between the *lac1* natural mutant ($lac1^{mutant}$) and the teosinte near isogenic line (NIL) for *RAVL1* ($RAVL1^{teosinte}$). $lac1^{W22}\,RAVL1^{W22}$ carries a W22 allele at *lac1* and *RAVL1*; $lac1^{W22}\,RAVL1^{teosinte}$ carries a W22 allele at *lac1* and a teosinte allele at *RAVL1*; $lac1^{mutant}\,RAVL1^{W22}$ carries a mutant allele at *lac1* and a W22 allele at *RAVL1*; $lac1^{mutant}\,RAVL1^{teosinte}$ carries a mutant allele at *lac1* and a teosinte allele at *RAVL1*. **b**,**c** Field trials for the four genotype combinations of *lac1* and *RAVL1* conducted in Tongzhou in 2023 (**b**) and in Sanya in 2023 (**c**). Data are mean ± s.d. (n = 3 biological replicates in a split-plot design). Different letters indicate statistically significant differences ($P < 0.05$, PROC MIXED with Fisher's Least Significant Difference test in SAS).

o

Experiment	1	2	3	4
Agrobacteriun-infected embryos	185	203	168	230
phosphinothricin-resistant calli transferred to regeneration medium	64	87	55	90
Number of PCR-positive regeneration events	4	8	4	10
The rate of bar resistant calli （%）	34.59	42.86	32.74	39.13
The rate of PCR-positive regeneration events （%）	6.25	9.20	7.27	11.11
The transformation efficiency （%）	2.16	3.94	2.38	4.35
Average transformation frequency （%）			3.21	

p

Inbred lines	D_0 haploids	D_0 plants carrying homozygous wild-type allele in *lac1*	D_0 plants carrying homozygous mutations in *lac1*	D_0 plants carrying heterozygous or mosaic mutations in *lac1*
43	1175	767	80 (6.8%)	328 (27.9%)

Extended Data Fig. 10 | See next page for caption.

Extended Data Fig. 10 | Different stages of *Agrobacterium*-mediated genetic transformation of the maize haploid-inducer line HI3. a, Donor material. HI3 ears were harvested 12–15 d after pollination, and immature embryos, around 1.5 mm in size, were isolated from maize kernels. **b**, *Agrobacterium* inoculation. Isolated immature embryos were collected in 1 mL of infection medium used for *Agrobacterium* inoculation. **c**, Immature-embryo co-cultivation. Immature embryos with scutellum-surface up were transferred to the surface of co-cultivation medium and incubated in the dark for 2-3 d. **d**, Immature embryos transiently expressing the GUS reporter gene. **e**-**g**, Selection cultivation. Immature embryos were transferred to the first selection medium and incubated in the dark for 10–12 days (**e**), and only pieces of embryogenic callus were cultured on the second selection medium for approximately 2 weeks (**f** and **g**). **h**, Regeneration cultivation. The embryogenic-resistant calli were transferred to regeneration medium and placed in 18 h light–6 h dark light regime for 3 weeks. **i**, Shoot growth. Green shoots with or without roots were transferred into culture tubes with shoot medium and grown under a 18 h light–6 h dark light regime for 2 weeks. **j**,**k**, Transplanting to soil of T_0 plants. T_0 transgenic individuals rooted in the soil in an acclimation room (**j**), and T_0 transgenic plants were transplanted to soil in the greenhouse (**k**). **l**-**n**, Flowering and pollination of T_0 transgenic plants (**l** and **m**), and T_1 seeds were harvested after 30 days pollination. **o**, Regeneration and transformation efficiencies of HI3 in four experiments. The rate of phosphinothricin-resistant calli was calculated as the number of phosphinothricin-resistant calli at regeneration divided by the number of infected embryos. The rate of PCR-positive regeneration events was calculated as the number of PCR-positive regeneration events divided by the number of phosphinothricin-resistant calli transferred to regeneration mediun. The transformation efficiency was calculated as the number of PCR-positive regeneration events divided by the number of infected embryos. **p**, Summary of haploid induction editing using HI3 carrying a gene-editing cassette targeting *lac1*.

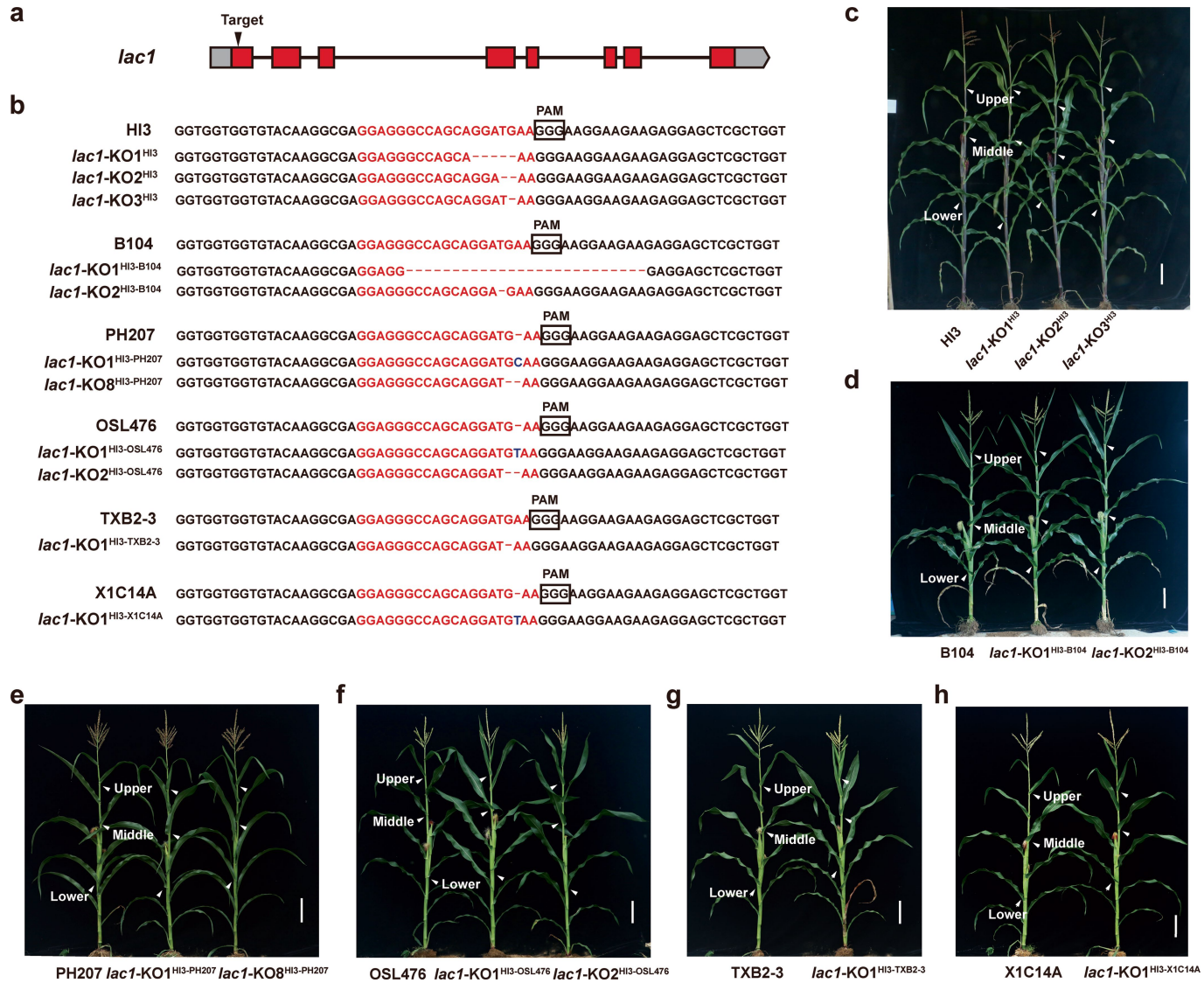

Extended Data Fig. 11 | Editing different maize inbred lines using HI3 carrying a gene-editing cassette targeting *lac1*. **a**, The target site in *lac1* used for haploid-induction editing. **b**, Sequence comparison of edited HI3 and edited doubled haploids from B104, PH207, OSL476, TXB2-3 and X1C14A at the target site. The wild-type sequences are shown at the top. **c**, Plant phenotypes of the edited haploid-inducer lines (*lac1*-KO1^{HI3}, *lac1*-KO2^{HI3} and *lac1*-KO3^{HI3}) and the original haploid-inducer line (HI3). **d**, Plant phenotypes of B104 and the edited doubled haploids from B104 (*lac1*-KO1$^{HI3\text{-}B104}$ and *lac1*-KO2$^{HI3\text{-}B104}$). **e**, Plant phenotypes of PH207 and the edited doubled haploids from PH207 (*lac1*-KO1$^{HI3\text{-}PH207}$ and *lac1*-KO8$^{HI3\text{-}PH207}$). **f**, Plant phenotypes of OSL476 and the edited doubled haploids from OSL476 (*lac1*-KO1$^{HI3\text{-}OSL476}$ and *lac1*-KO2$^{HI3\text{-}OSL476}$). **g**, Plant phenotypes of TXB2-3 and the edited doubled haploid from TXB2-3 (*lac1*-KO1$^{HI3\text{-}TXB2\text{-}3}$). **h**, Plant phenotypes between X1C14A and the edited doubled haploid from X1C14A (*lac1*-KO1$^{HI3\text{-}X1C14A}$). In **c**-**h**, the white arrows indicate the lower, middle, and upper leaves from which leaf angle was scored. Scale bar = 18 cm.

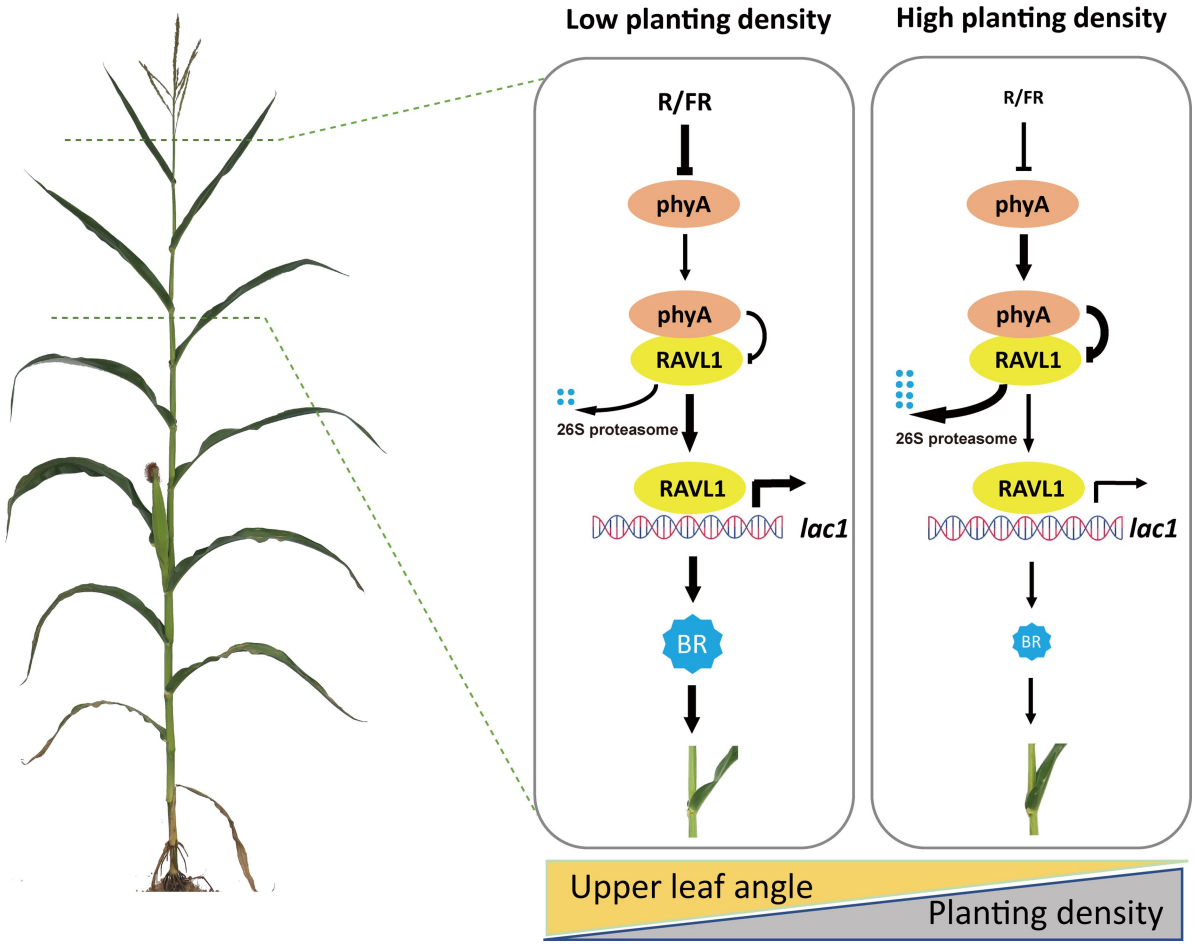

Extended Data Fig. 12 | Model for how *lac1* responds to varying light signals to dynamically regulate upper leaf angle as planting density increases. At high planting densities, neighbor proximity induces a low R:FR ratio perceived by the upper leaves. The phytochrome A (phyA) photoreceptors accumulate and physically interact with the transcription factor RAVL1 to promote the degradation of RAVL1 via the 26 S proteasome pathway, thus attenuating RAVL1-dependent activation of *lac1*. This consequently reduces brassinosteroid levels in the collar and ultimately decreases upper leaf angles at high planting densities. R:FR, red to far-red light ratio. BR, brassinosteroid. Figure was created with BioRender (https://biorender.com/).

nature portfolio

Corresponding author(s): Feng Tian, Jigang Li

Last updated by author(s): May 26, 2024

Reporting Summary

Nature Portfolio wishes to improve the reproducibility of the work that we publish. This form provides structure for consistency and transparency in reporting. For further information on Nature Portfolio policies, see our Editorial Policies and the Editorial Policy Checklist.

Statistics

For all statistical analyses, confirm that the following items are present in the figure legend, table legend, main text, or Methods section.

n/a	Confirmed	
☐	☒	The exact sample size (*n*) for each experimental group/condition, given as a discrete number and unit of measurement
☐	☒	A statement on whether measurements were taken from distinct samples or whether the same sample was measured repeatedly
☐	☒	The statistical test(s) used AND whether they are one- or two-sided *Only common tests should be described solely by name; describe more complex techniques in the Methods section.*
☒	☐	A description of all covariates tested
☐	☒	A description of any assumptions or corrections, such as tests of normality and adjustment for multiple comparisons
☐	☒	A full description of the statistical parameters including central tendency (e.g. means) or other basic estimates (e.g. regression coefficient) AND variation (e.g. standard deviation) or associated estimates of uncertainty (e.g. confidence intervals)
☐	☒	For null hypothesis testing, the test statistic (e.g. *F*, *t*, *r*) with confidence intervals, effect sizes, degrees of freedom and *P* value noted *Give P values as exact values whenever suitable.*
☒	☐	For Bayesian analysis, information on the choice of priors and Markov chain Monte Carlo settings
☒	☐	For hierarchical and complex designs, identification of the appropriate level for tests and full reporting of outcomes
☐	☒	Estimates of effect sizes (e.g. Cohen's *d*, Pearson's *r*), indicating how they were calculated

Our web collection on statistics for biologists contains articles on many of the points above.

Software and code

Policy information about availability of computer code

Data collection	Hitachi FE-SEM Field Emission Scanning Electron Microscope, S-4700 (scanning electron microscopy); ImageJ 1.54d (ligular width, cell length and width, and protein levels); OLYMPUS CX23, and ToupView (histological analysis); Applied Biosystems 7500 (RT-qPCR); ChemiScope6000 (immunoblot image); Tanon-5200 (the split firefly luciferase complementation assays); Thermo Scientific Ultimate 3000 UHPLC coupled with TSQ Quantiva (endogenous brassinosteroid contents); LI-1500 Light Sensor Logger (photosynthetically active radiation); LI-COR 6400XT instrument (photosynthesis of maize plants).
Data analysis	SAS v.9.2 (ANOVA, PROC Mixed); Microsoft Excel 2010 (two-sided Students' test); R v4.0.1 (Correlation analysis); MEGA 6.06 (phylogenetic analysis); BioEdit 7.0.9.1 (Sequence aligment).

For manuscripts utilizing custom algorithms or software that are central to the research but not yet described in published literature, software must be made available to editors and reviewers. We strongly encourage code deposition in a community repository (e.g. GitHub). See the Nature Portfolio guidelines for submitting code & software for further information.

Data

Policy information about availability of data

All manuscripts must include a data availability statement. This statement should provide the following information, where applicable:

- Accession codes, unique identifiers, or web links for publicly available datasets
- A description of any restrictions on data availability
- For clinical datasets or third party data, please ensure that the statement adheres to our policy

Provide your data availability statement here.

Research involving human participants, their data, or biological material

Policy information about studies with human participants or human data. See also policy information about sex, gender (identity/presentation), and sexual orientation and race, ethnicity and racism.

Reporting on sex and gender	NA
Reporting on race, ethnicity, or other socially relevant groupings	NA
Population characteristics	NA
Recruitment	NA
Ethics oversight	NA

Note that full information on the approval of the study protocol must also be provided in the manuscript.

Field-specific reporting

Please select the one below that is the best fit for your research. If you are not sure, read the appropriate sections before making your selection.

☒ Life sciences ☐ Behavioural & social sciences ☐ Ecological, evolutionary & environmental sciences

For a reference copy of the document with all sections, see nature.com/documents/nr-reporting-summary-flat.pdf

Life sciences study design

All studies must disclose on these points even when the disclosure is negative.

Sample size	No statistical methods were used to predetermine sample size. The sample size and the results of statistical analyses were described in the relevant figures or method section. Required experimental sample sizes were estimated based on past experience performing similar experiments and previously published results (Tian et al, Science 365:658-664).
Data exclusions	No data was excluded from the analyses.
Replication	All molecular experiments in this study were repeated independently at least three times. A split-plot design with three replications was used in all field trials. Plant densities were randomized in the main plots and genotypes were subplots. Related information is indicated in figure legends.
Randomization	Samples of the same genotypes were randomly collected.
Blinding	The research materials are edited plants, which need to be strictly regulated and clearly labeled during the experimental process, so the blinding design is not applicable to this system, field trials were designed with three replicates in four locations over four years under regular and high planting densities.

Reporting for specific materials, systems and methods

We require information from authors about some types of materials, experimental systems and methods used in many studies. Here, indicate whether each material, system or method listed is relevant to your study. If you are not sure if a list item applies to your research, read the appropriate section before selecting a response.

Materials & experimental systems

n/a	Involved in the study
☐	☒ Antibodies
☒	☐ Eukaryotic cell lines
☒	☐ Palaeontology and archaeology
☒	☐ Animals and other organisms
☒	☐ Clinical data
☒	☐ Dual use research of concern
☐	☒ Plants

Methods

n/a	Involved in the study
☒	☐ ChIP-seq
☒	☐ Flow cytometry
☒	☐ MRI-based neuroimaging

Antibodies

Antibodies used

anti-RAVL1 antibody (made by Shanghai Youke Biotechnology Co., Ltd, 1:1500); anti-phyA antibody (made by Beijing Protein Innovation, 1:1000); anti-ACTIN (ABclonal Technology, Cat. NO: AC009, 1:8000); anti-HSP82 (Beijing Protein Innovation, CATALOG # AbM51099-31-PU, 1:6000); anti-His (YEASEN, CAT:30401ES80, 1:6000); anti-GST (ABclonal Technology, Cat. NO: AE001, 1:6000); anti-MYC (MBL, M047-3, 1: 6000); anti-GFP (TransGen, HT801, 1:6000).

Validation

Residues 192–206 of RAVL1 was used to make antibodies by Shanghai Youke Biotechnology Co., Ltd, and WT and RAVL1-KO1 were used to validate anti-RAVL1 antibody. His-phyA1-C protein was used to make antibodies by Beijing Protein Innovation, and WT and phyA-KO1 was used to validate anti-phyA antibody. The antibodies of ACTIN, HSP82, His-tag, GST, MYC and GFP are commercially available from the manufacturer.
Anti-ACTIN antibody manufacturer's website: https://abclonal.com.cn/catalog/AC009
Anti-HSP82 antibody manufacturer's website: http://www.proteomics.org.cn/product/202.html
Anti-His-tag antibody manufacturer's website: https://www.yeasen.com/products/detail/888
Anti-GST antibody manufacturer's website: https: //abclonal.com.cn/catalog/AE001
Anti-MYC antibody manufacturer's website: http://www.mbl-chinawide.cn/search012?keyword=M047-3
Anti-GFP antibody manufacturer's website: https://www.transgen.com/antibody_tag/390.html

Dual use research of concern

Policy information about dual use research of concern

Hazards

Could the accidental, deliberate or reckless misuse of agents or technologies generated in the work, or the application of information presented in the manuscript, pose a threat to:

No	Yes
☒	☐ Public health
☒	☐ National security
☒	☐ Crops and/or livestock
☒	☐ Ecosystems
☒	☐ Any other significant area

Experiments of concern

Does the work involve any of these experiments of concern:

No	Yes
☒	☐ Demonstrate how to render a vaccine ineffective
☒	☐ Confer resistance to therapeutically useful antibiotics or antiviral agents
☒	☐ Enhance the virulence of a pathogen or render a nonpathogen virulent
☒	☐ Increase transmissibility of a pathogen
☒	☐ Alter the host range of a pathogen
☒	☐ Enable evasion of diagnostic/detection modalities
☒	☐ Enable the weaponization of a biological agent or toxin
☒	☐ Any other potentially harmful combination of experiments and agents

Plants

Seed stocks

lac1 is a naturally occurred mutant initially discovered in a population of maize inbred line W22 genetic background. The knockout lines for lac1, D11 and the phyA1 phyA2 double mutants were generated in the LH244 background. The lac1 overexpression lines were generated in the B104 background.

Novel plant genotypes

The CRISPR-Cas9 technique was used to generate knockout lines for lac1, D11 and phyA. The endogenous sequences targeted for editing, the number of independent transgenic events and the edited sites were indicated in figures or figure legends, and Agrobacterium-mediated transformation using maize immature embryos was performed to generate transgenic plants.

Authentication

Primers used for genotyping lac1 were provided in Supplementary Table 1. The target sequences for lac1, D11 and phyA genes were individually designed and cloned into the pBUE411 vector under the control of the maize Ubiquitin 1 promoter, and then transformed to the maize inbred line LH244 to generate lac1, D11 and phyA knockout lines respectively. The lac1 and D11 double mutants were generated by crossing lac1-KO2 and D11-KO1/D11-KO2. The full-length coding sequence of lac1 was cloned into pCAMBIA3300-GFP and transformed to the maize inbred line B104 to generate lac1-OE1 and lac1-OE2. The CRISPR–Cas9 cassette targeting lac1 was transformed into HI3. The HI3 plants carrying the CRISPR–Cas9 cassette targeting lac1 were crossed with different maize inbred lines to generate gene-edited haploids in these inbred line backgrounds. The gene-edited haploids were then doubled using the mitotic inhibitor colchicine. Sanger sequencing was used to identify knockout lines and overexpressing lines, and primers were provided in Supplementary Table 4.